**Supplementary information**

# The protein circPETH-147aa regulates metabolic reprogramming in hepatocellular carcinoma cells to remodel immunosuppressive microenvironment

Tian Lan, Fengwei Gao, Yunshi Cai, Yinghao Lv, Jiang Zhu, Hu Liu, Sinan Xie, Haifeng Wan, Haorong He, Kunlin Xie, Chang Liu, and Hong Wu

**Supplementary Figures**

**Supplementary Fig. 1: TAMs promote the invasion, migration and aerobic glycolysis of HCC cells, related to Fig. 1.**

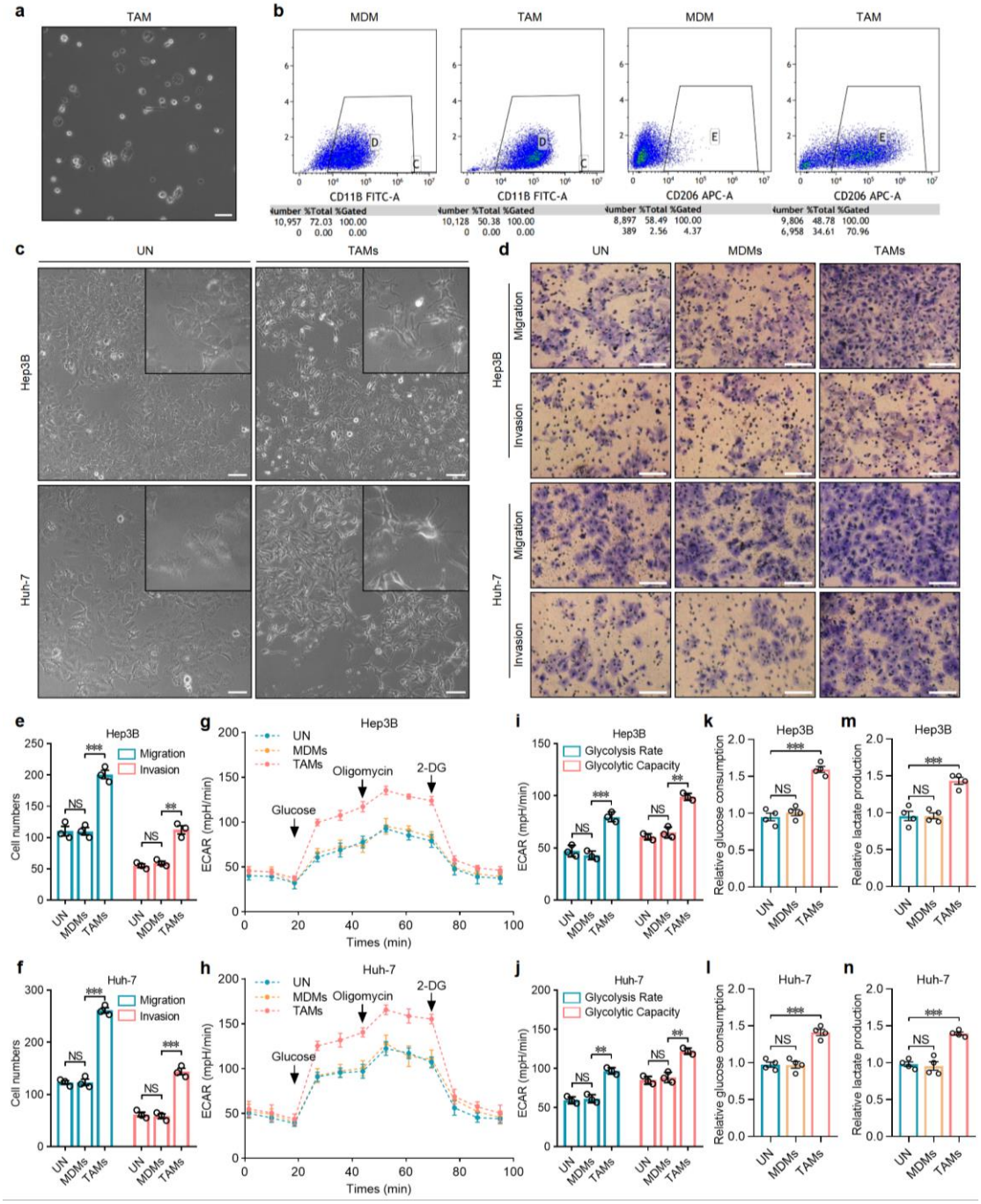


**a,** Phase-contrast micrograph of TAMs isolated from human HCC tissues. Scale bar, 50 μm. **b,** Flow cytometry analysis of CD11b and CD206 expression on TAMs and MDMs. **c,** Phase-contrast micrographs of Hep3B and Huh-7 cells cocultured with TAMs without physical interaction for 72 h. Boxes indicate the areas with higher magnification shown at the upper right corner. Scale bar, 50 μm. **d,** The invasion and

migration of Hep3B and Huh-7 cells cocultured with TAMs or MDMs. Scale bar, 100 μm. **e,f,** Quantification of the invasion and migration of Hep3B and Huh-7 cells cocultured with TAMs or MDMs. $n = 3$ independent experiments. Data are shown as mean ± SEM. Exact *P* values from left to right (**e**): 0.000552, 0.001752. Exact *P* values from left to right (**f**): 6.71E−05, 0.000348. **g,h,** ECARs of Hep3B and Huh-7 cells cocultured with TAMs or MDMs. **i,j,** Glycolysis rates and glycolysis capacities of Hep3B and Huh-7 cells cocultured with TAMs or MDMs. $n = 3$ independent experiments. Data are shown as mean ± SEM. Exact *P* values from left to right (**i**): 0.000979, 0.001731. Exact *P* values from left to right (**j**): 0.001469, 0.002405. **k,l,** Glucose consumption of Hep3B and Huh-7 cells cocultured with TAMs or MDMs. $n = 4$ independent experiments. Data are shown as mean ± SEM. Exact *P* value (**k**): 6.52E−05. Exact *P* value (**l**): 0.000204. **m,n,** Lactate production of Hep3B and Huh-7 cells cocultured with TAMs or MDMs. $n = 4$ independent experiments. Data are shown as mean ± SEM. Exact *P* value (**m**): 0.000930. Exact *P* value (**n**): 3.52E−05. NS, not significant; ***, $P < 0.001$ by two-tailed Student's T-test. Data are representative of at least three independent experiments.

**Supplementary Fig. 2: EVs mediate the effects of TAMs by enhancing the acquisition of the metastatic and metabolic phenotypes by HCC cells, related to Fig. 1.**

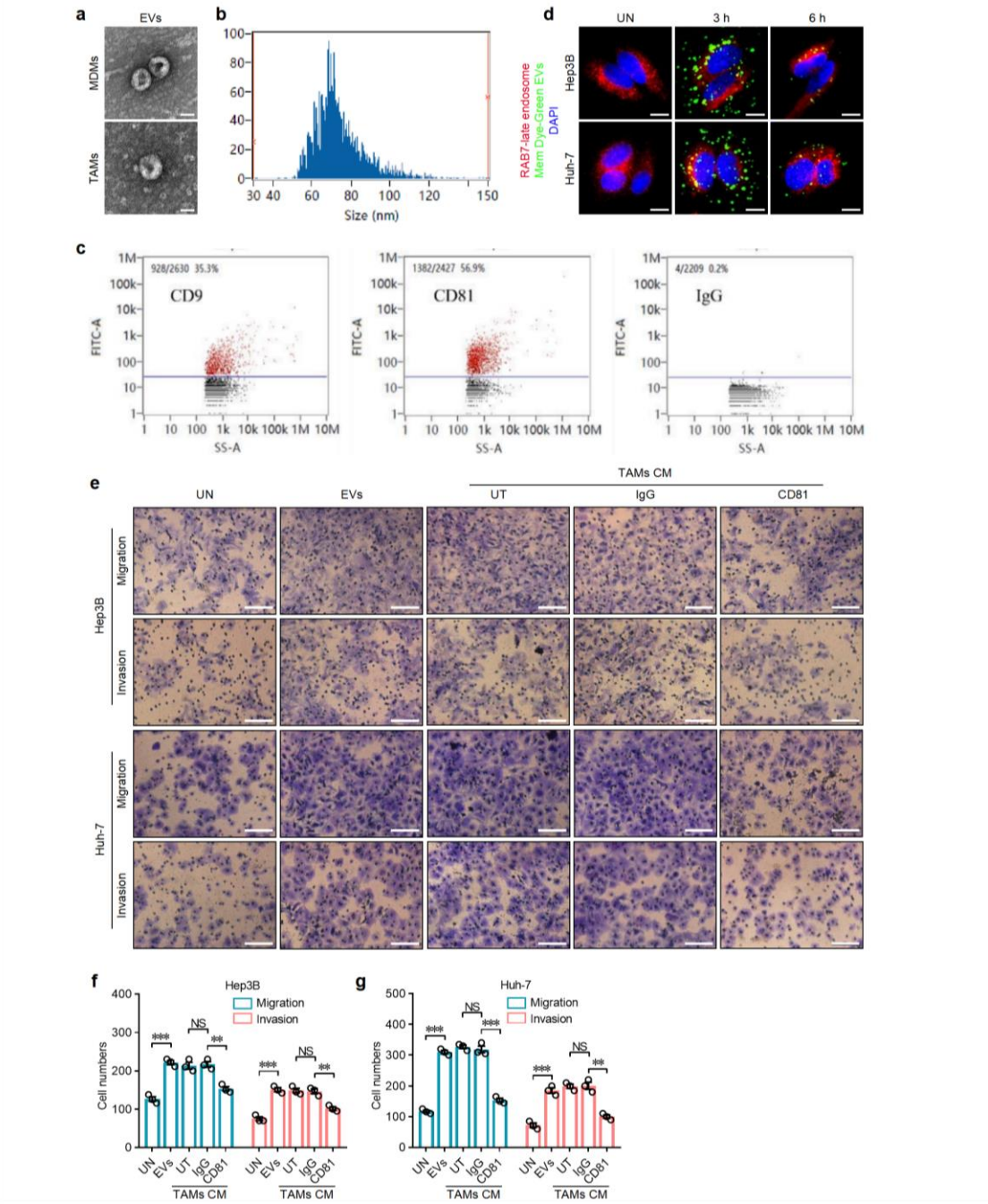


**a,** Representative transmission electron microscopy image of EVs isolated from TAMs and MDMs CM. Scale bar, 50 nm. **b,** Particle diameter of EVs was determined by nanoparticle tracking system. **c,** NanoFCM analysis of CD9 and CD81 expression on EVs. **d,** Representative confocal microscopy images of Hep3B and Huh-7 cells treated with Mem Dye-Green-labelled TAMs EVs for 3 h and 6 h. Colocalization of EVs and

$RAB7^+$ late endosome was observed 6 h after the treatment. Scale bar, 10 μm. **e,** The invasion and migration of Hep3B and Huh-7 cells treated with EVs or TAMs CM. A neutralizing antibody against CD81 was used to deplete EVs in TAMs CM. Scale bar, 100 μm. **f,g,** Quantification of the invasion and migration of Hep3B and Huh-7 cells treated with EVs or TAMs CM. A neutralizing antibody against CD81 was used to deplete EVs in TAMs CM. $n = 3$ independent experiments. Data are shown as mean ± SEM. Exact *P* values from left to right (**f**): 0.000358, 0.002557, 0.000468, 0.003795. Exact *P* values from left to right (**g**): 1.17E−05, 0.000189, 0.000556, 0.001496. NS, not significant; **, $P < 0.01$; ***, $P < 0.001$ by two-tailed Student's T-test. Data are representative of at least three independent experiments.

**Supplementary Fig. 3: Identification of circPETH and its correlation with the prognosis of HCC patients, related to Fig. 1.**

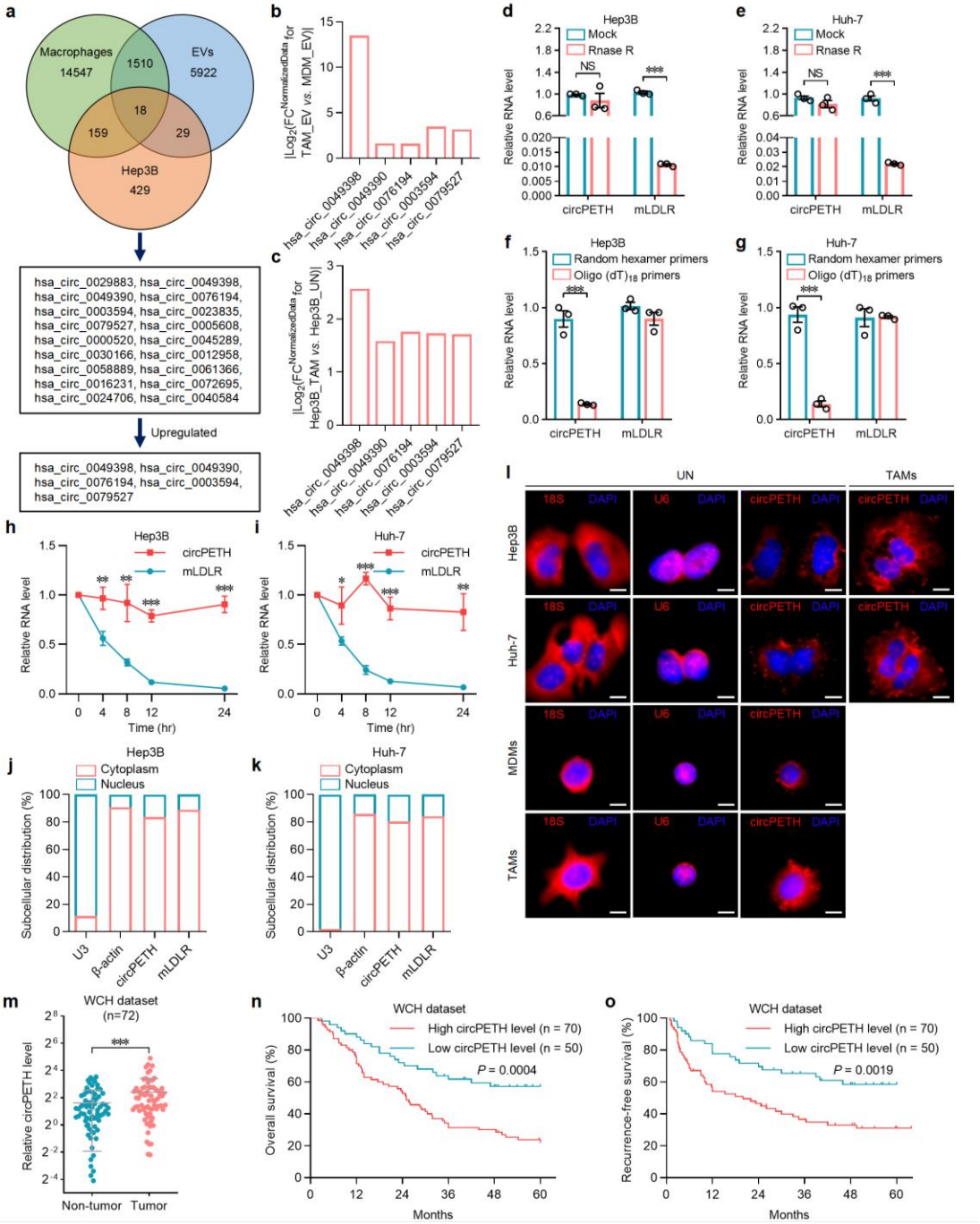


**a,** Schematic of the selection for the circRNAs packaged by EVs and transmitted from TAMs to HCC cells. **b,** Microarray data of the fold change of candidate circRNAs in EVs from TAMs compared with those from MDMs. **c,** Microarray data of the fold change of candidate circRNAs in Hep3B cells cocultured with TAMs compared with those cultured alone. **d,e,** qRT-PCR for the relative expressions of circPETH and mLDLR after treatment with RNase R in Hep3B and Huh-7 cells. $n = 3$ independent

experiments. Data are shown as mean ± SEM. Exact *P* value (**d**): 1.94E−06. Exact *P* value (**e**): 4.02E−05. **f,g,** Random hexamer or oligo $(dT)_{18}$ primers were used in the reverse transcription experiments. The relative RNA levels were evaluated by qRT-PCR. $n = 3$ independent experiments. Data are shown as mean ± SEM. Exact *P* value (**f**): 0.000476. Exact *P* value (**g**): 0.000413. **h,i,** The relative RNA levels of circPETH and mLDLR accessed by qRT-PCR after treatment with Actinomycin D at the indicated time points in Hep3B and Huh-7 cells. $n = 3$ independent experiments. Data are shown as mean ± SEM. Exact *P* values from left to right (**h**): 0.006377, 0.005407, 5.71E−05, 5.76E−05. Exact *P* values from left to right (**i**): 0.032153, 3.18E−05, 0.000409, 0.002051. **j,k,** Cytoplasmic and nucleus fraction assay showing that circPETH and mLDLR mainly localized in cytoplasm of Hep3B and Huh-7 cells. β-actin and U3 were used as positive controls in the cytoplasm and nucleus, respectively. **l,** RNA fluorescence in situ hybridization showing cytoplasmic localization of circPETH and relative expression of circPETH in Hep3B and Huh-7 cells cocultured with TAMs. The 18S and U6 were applied as positive controls in the cytoplasm and nucleus. Scale bar, 10 μm. **m,** circPETH expression in 72 matched HCC and adjacent normal samples from WCH dataset by using qRT-PCR. Data are shown as mean ± SD. Exact *P* value: 0.000582. **n,o,** Kaplan-Meier analyses of the correlations between circPETH expression and overall survival or recurrence-free survival of 120 HCC patients. The cutoff value was determined by X-tile. $n = 70$ for high circPETH group and $n = 50$ for low circPETH group. *P* values were determined by log-rank tests. NS, not significant; *, $P < 0.05$; **, $P < 0.01$; ***, $P < 0.001$ by two-tailed Student's T-test. Data are representative of at least three independent experiments.

**Supplementary Fig. 4: ADAR1 inhibits the pairing of I12RC and I15RC sequences and restrains the circularization of circPETH, related to Fig. 1.**

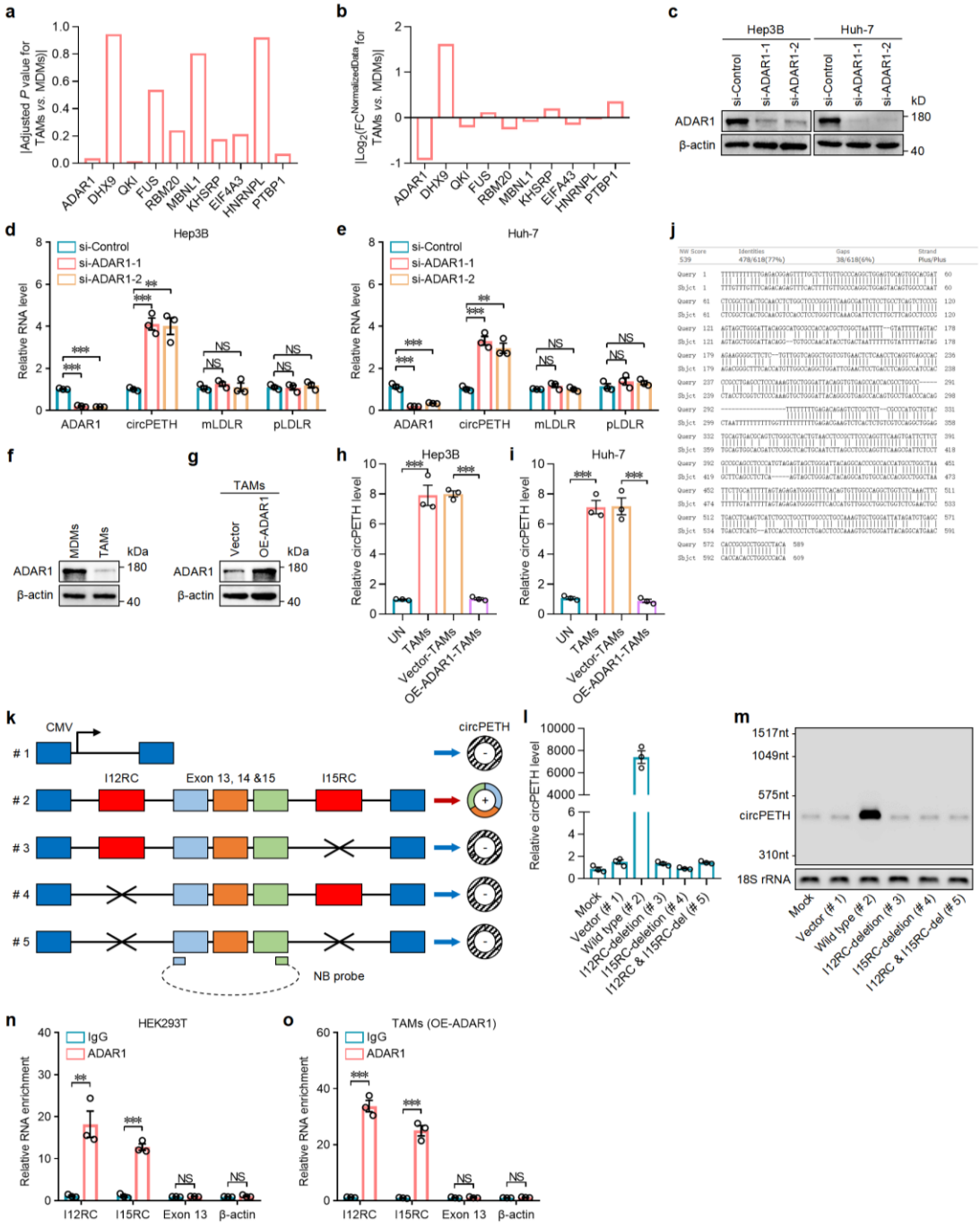


**a,** Microarray data of adjusted *P* value of candidate RBPs in TAMs compared with those in MDMs. **b,** Microarray data of the fold change of candidate RBPs in TAMs compared with those in MDMs. **c,** ADAR1 expression in Hep3B and Huh-7 cells with ADAR1 knockdown by western blot. The samples derive from the same experiment but different gels for ADAR1, and another for β-actin were processed in parallel. **d,e,** The expressions of ADAR1, circPETH, mLDLR and pLDLR in Hep3B and Huh-7 cells

with ADAR1 knockdown by qRT-PCR. $n = 3$ independent experiments. Data are shown as mean ± SEM. Exact *P* values from top to bottom and left to right (**d**): 2.60E−06, 1.18E−05, 0.001666, 0.000411. Exact *P* values from top to bottom and left to right (**e**): 0.000673, 0.000332, 0.001448, 0.000455. **f,** ADAR1 expression in TAMs and MDMs by western blot. **g,** ADAR1 expression in TAMs with ADAR1 overexpression by western blot. **h,i,** circRNA expression in Hep3B and Huh-7 cells cocultured with indicated TAMs by qRT-PCR. $n = 3$ independent experiments. Data are shown as mean ± SEM. Exact *P* values from left to right (**h**): 0.000506, 4.90E−06. Exact *P* values from left to right (**i**): 0.000179, 0.000380. **j,** The sequence of intron 12 was aligned to that of intron 15 of the LDLR gene by using BLAST (https://blast.ncbi.nlm.nih.gov/Blast.cgi). Highly reverse complementary sequences (77% identity over 618 nucleotides) were found and named as I12RC (reverse complementary sequences in intron 12) and I15RC (reverse complementary sequences in intron 15), respectively. **k,** Schematic of five different vectors (#1 to #5). The genomic region for circPETH (exon 13-15) with its wild-type flanking inverted complementary sequences (red boxes) was inserted into vector (#2). #3 to #5 represent a series of deletions of flanking inverted complementary sequences. The northern blot (NB) probe targeting circPETH is indicated by the dotted line. **l,m,** circPETH expression in HEK293T cells transfected with these five vectors by qRT-PCR and northern blot. **n,o,** The enrichments of I12RC and I15RC in ADAR1-immunoprecipitated RNAs for HEK293T cells and TAMs with ADAR1 overexpression by RIP assays. $n = 3$ independent experiments. Data are shown as mean ± SEM. Exact *P* values from left to right (**n**): 0.005474, 0.000160. Exact *P* values from left to right (**o**): 9.13E−05, 0.000214. NS, not significant; **, $P < 0.01$; ***, $P < 0.001$ by two-tailed Student's T-test. Data are representative of at least three independent experiments.

**Supplementary Fig. 5: Knockdown of circPETH suppresses the invasion and migration of HCC cells, related to Fig. 1.**

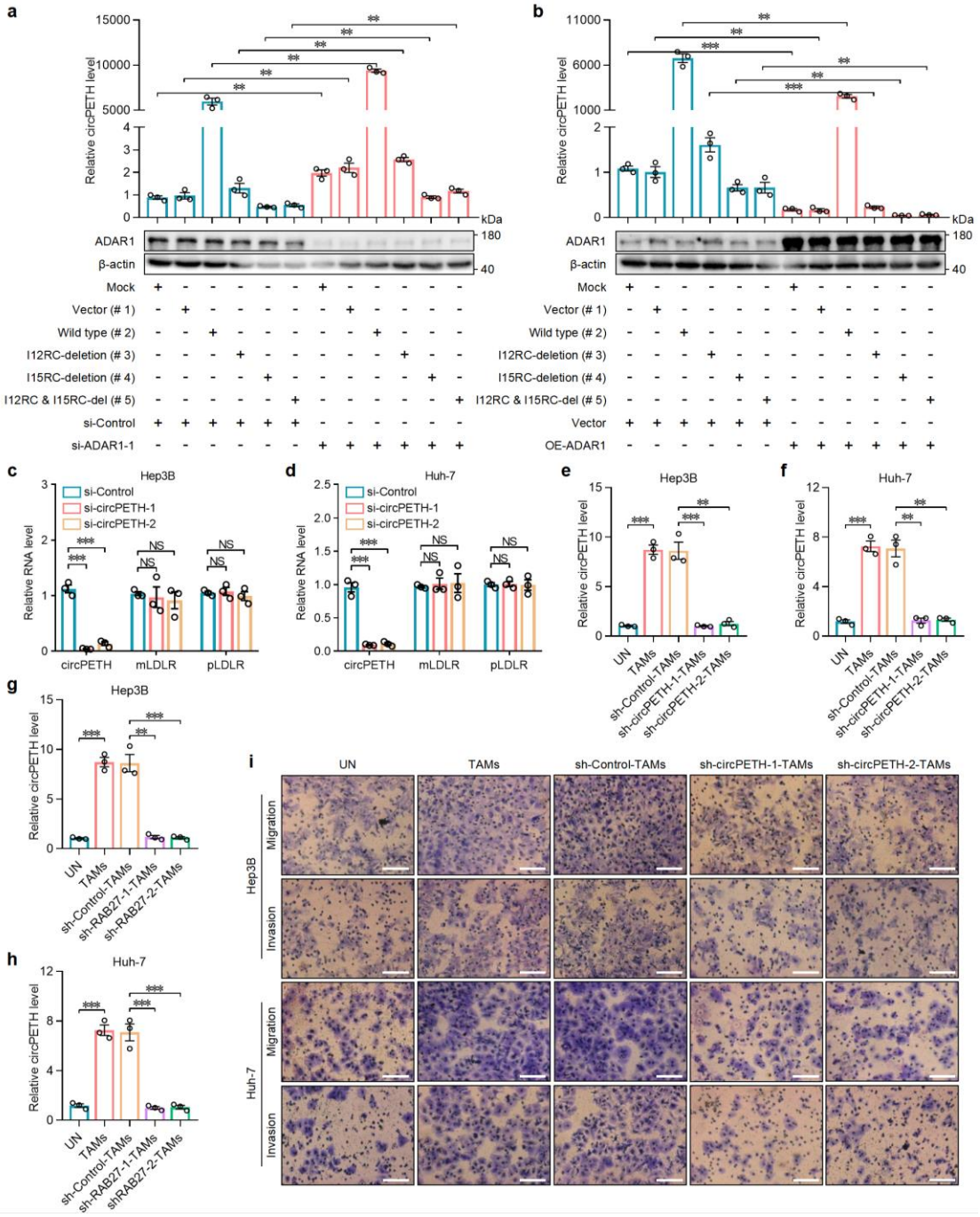


**a,b,** circPETH expression in HEK293T cells co-transfected with five vectors and ADAR1 siRNA-1 or overexpression plasmid by qRT-PCR. The samples derive from the same experiment but different gels for ADAR1, and another for β-actin were processed in parallel. $n = 3$ independent experiments. Data are shown as mean ± SEM. Exact *P* values from top to bottom (**a**): 0.003819, 0.001961, 0.005493, 0.001178, 0.007407, 0.002449. Exact *P* values from top to bottom (**b**): 0.001318, 0.002379,

0.000108, 0.007066, 0.001007, 0.000994. **c,d,** The expressions of circPETH, mLDLR and pLDLR in Hep3B and Huh-7 cells transfected with circPETH siRNAs by qRT-PCR. $n = 3$ independent experiments. Data are shown as mean ± SEM. Exact *P* values from top to bottom (**c**): 0.000213, 0.000101. Exact *P* values from top to bottom (**d**): 0.000309, 0.000249. **e-h,** circRNA expression in Hep3B and Huh-7 cells cocultured with indicated TAMs by qRT-PCR. $n = 3$ independent experiments. Data are shown as mean ± SEM. Exact *P* values from left to right and top to bottom (**e**): 8.48E−05, 0.001175, 0.000930. Exact *P* values from left to right and top to bottom (**f**): 0.000167, 0.001128, 0.001197. Exact *P* values from left to right and top to bottom (**g**): 8.48E−05, 0.000992, 0.001065. Exact *P* values from left to right and top to bottom (**h**): 0.000167, 0.000969, 0.000896. **i,** The invasion and migration of Hep3B and Huh-7 cells cocultured with indicated TAMs. Scale bar, 100 μm. NS, not significant; **, $P < 0.01$; ***, $P < 0.001$ by two-tailed Student's T-test. Data are representative of at least three independent experiments.

**Supplementary Fig. 6: Both knockdown and knockout of circPETH inhibit the invasion, migration and aerobic glycolysis of HCC cells, related to Fig. 1.**

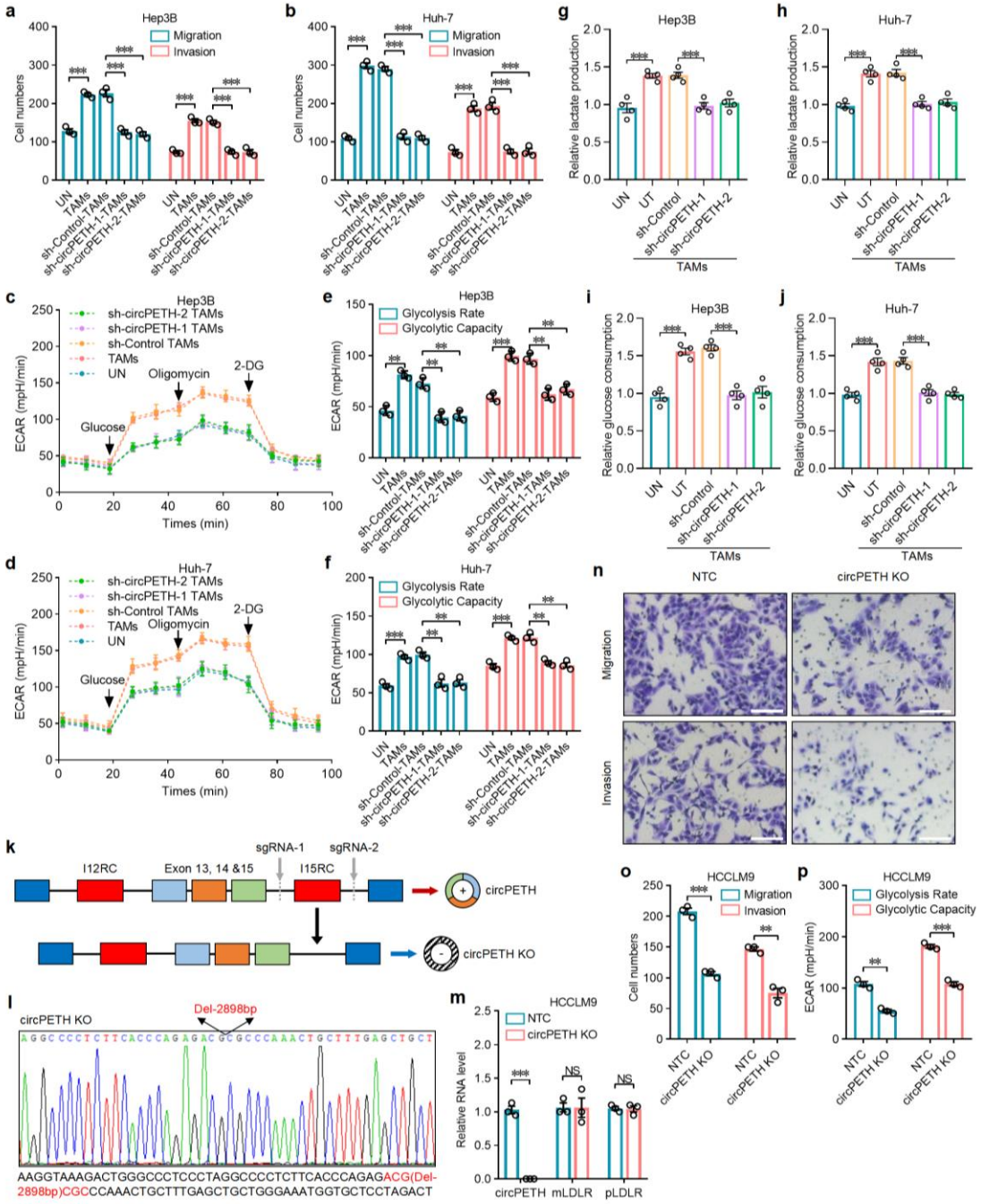


**a,b,** Quantification of the invasion and migration of Hep3B and Huh-7 cells cocultured with indicated TAMs. $n = 3$ independent experiments. Data are shown as mean ± SEM. Exact *P* values from left to right and top to bottom (**a**): 0.000219, 0.000537, 0.000646, 0.000170, 0.000464, 0.000231. Exact *P* values from left to right and top to bottom (**b**): 2.54E−05, 2.51E−05, 4.48E−05, 0.000275, 0.000532, 0.000359. **c,d,** ECARs of Hep3B and Huh-7 cells cocultured with indicated TAMs. **e,f,** Glycolysis rates and glycolysis

capacities of Hep3B and Huh-7 cells cocultured with indicated TAMs. $n = 3$ independent experiments. Data are shown as mean ± SEM. Exact *P* values from left to right and top to bottom (**e**): 0.001199, 0.003372, 0.003050, 0.000189, 0.004136, 0.002900. Exact *P* values from left to right and top to bottom (**f**): 0.000864, 0.002757, 0.002789, 0.000847, 0.003578, 0.006463. **g,h,** Lactate production of Hep3B and Huh-7 cells cocultured with indicated TAMs. $n = 4$ independent experiments. Data are shown as mean ± SEM. Exact *P* values from left to right (**g**): 0.000926, 0.000552. Exact *P* values from left to right (**h**): 0.000181, 0.000270. **i,j,** Glucose consumption of Hep3B and Huh-7 cells cocultured with indicated TAMs. $n = 4$ independent experiments. Data are shown as mean ± SEM. Exact *P* values from left to right (**i**): 9.87E−05, 0.000107. Exact *P* values from left to right (**j**): 0.000371, 0.000389. **k,** The CRISPR–Cas9 strategy for KO I15RC sequence to block the circularization of circPETH. **l,** Sanger sequencing of CRISPR–Cas9-induced circPETH KO in HCCLM9 cells. **m,** The expressions of circPETH, mLDLR and pLDLR in HCCLM9 cells with circPETH KO by qRT-PCR. $n = 3$ independent experiments. Data are shown as mean ± SEM. Exact *P* value: 4.7E−05. **n,** The invasion and migration of HCCLM9 cells with circPETH KO. Scale bar, 100 μm. **o,** Quantification of the invasion and migration of HCCLM9 cells with circPETH KO. $n = 3$ independent experiments. Data are shown as mean ± SEM. Exact *P* values from left to right: 8.49E−05, 0.001005. **p,** Glycolysis rate and glycolysis capacity of HCCLM9 cells with circPETH KO. $n = 3$ independent experiments. Data are shown as mean ± SEM. $n = 3$ independent experiments. Data are shown as mean ± SEM. Exact *P* values from left to right: 0.001380, 0.000409. NS, not significant; **, $P < 0.01$; ***, $P < 0.001$ by two-tailed Student's T-test. Data are representative of at least three independent experiments.

**Supplementary Fig. 7: Effects of circPETH KO on metastasis of HCC cells and a positive feedback loop formed by circPETH, ADAR1 and lactate, related to Fig. 2.**

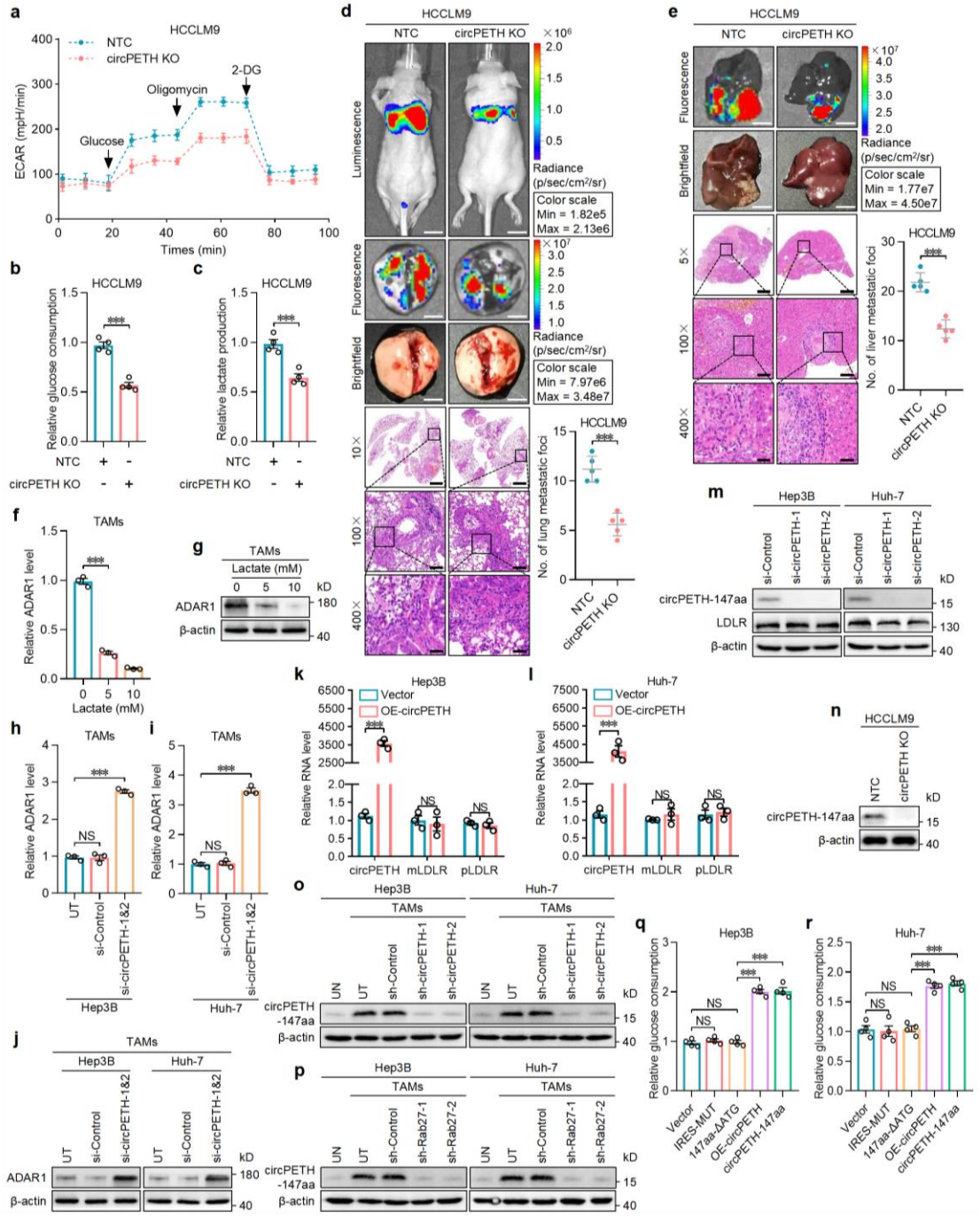


**a,** ECARs of HCCLM9 cells with circPETH KO. **b,** Glucose consumption of HCCLM9 cells with circPETH KO. $n = 4$ independent experiments. Data are shown as mean ± SEM. Exact *P* value: 9.89E−05. **c,** Lactate production of HCCLM9 cells with circPETH KO. $n = 4$ independent experiments. Data are shown as mean ± SEM. Exact *P* value: 0.000457. **d,** Top: Representative bioluminescence photographs of the murine tail vein injection lung metastasis models with indicated HCCLM9 cells.

Middle: Representative fluorescence and brightfield photographs of pulmonary metastatic nodules in lung metastasis models with indicated HCCLM9 cells. Bottom: Representative HE staining and statistical analysis of metastatic foci in the lung. Scale bars from top to bottom: 1 cm, 4 mm, 4 mm, 2.8 mm, 280 μm, 70 μm. $n = 5$ for each group. Data are shown as mean ± SD. Exact *P* value: 8.98E−05. **e,** Top: Representative fluorescence and brightfield photographs of intrahepatic metastatic nodules in liver orthotopic implanted intrahepatic metastasis models. Bottom: Representative HE staining and statistical analysis of metastatic foci in the liver. Scale bars from top to bottom: 7.5 mm, 7.5 mm, 2.8 mm, 280 μm, 70 μm. $n = 5$ for each group. Data are shown as mean ± SD. Exact *P* value: 4.59E−05. **f,g,** ADAR1 expression in TAMs treated with lactate at different concentrations for 24 h by qRT-PCR and western blot. $n = 3$ independent experiments. Data are shown as mean ± SEM. Exact *P* value (**f**): 3.04E−05. **h-j,** ADAR1 expression in TAMs cocultured with indicated Hep3B and Huh-7 cells by qRT-PCR and western blot. $n = 3$ independent experiments. Data are shown as mean ± SEM. Exact *P* value (**h**): 1.02E−05. Exact *P* value (**i**): 1.64E−05. **k,l,** The expressions of circPETH, mLDLR and pLDLR in Hep3B and Huh-7 cells with circPETH overexpression by qRT-PCR. $n = 3$ independent experiments. Data are shown as mean ± SEM. Exact *P* value (**k**): 1.89E−05. Exact *P* value (**l**): 0.000181. **m,** The expressions of circPETH-147aa and LDLR in Hep3B and Huh-7 cells transfected with circPETH siRNAs by western blot. The samples derive from the same experiment but different gels for circPETH-147aa, another for LDLR and another for β-actin were processed in parallel. **n,** circPETH-147aa expression in HCCLM9 cells with circPETH KO by western blot. **o,p,** circRNA-147aa expression in Hep3B and Huh-7 cells cocultured with indicated TAMs by western blot. The samples derive from the same experiment but different gels for circPETH-147aa, and another for β-actin were processed in parallel. **q,r,** Glucose consumption of Hep3B and Huh-7 cells transfected with five different vectors. $n = 4$ independent experiments. Data are shown as mean ± SEM. Exact *P* values from top to bottom (**q**): 7.82E−06, 1.55E−06. Exact *P* values from top to bottom (**r**): 2.07E−05, 2.99E−05. NS, not significant; ***, $P < 0.001$ by two-tailed Student's T-test. Data are representative of at least three

independent experiments.

**Supplementary Fig. 8: Overexpression of circPETH-147aa or translatable circPETH reinforces the invasion, migration and aerobic glycolysis of HCC cells, related to Fig. 2.**

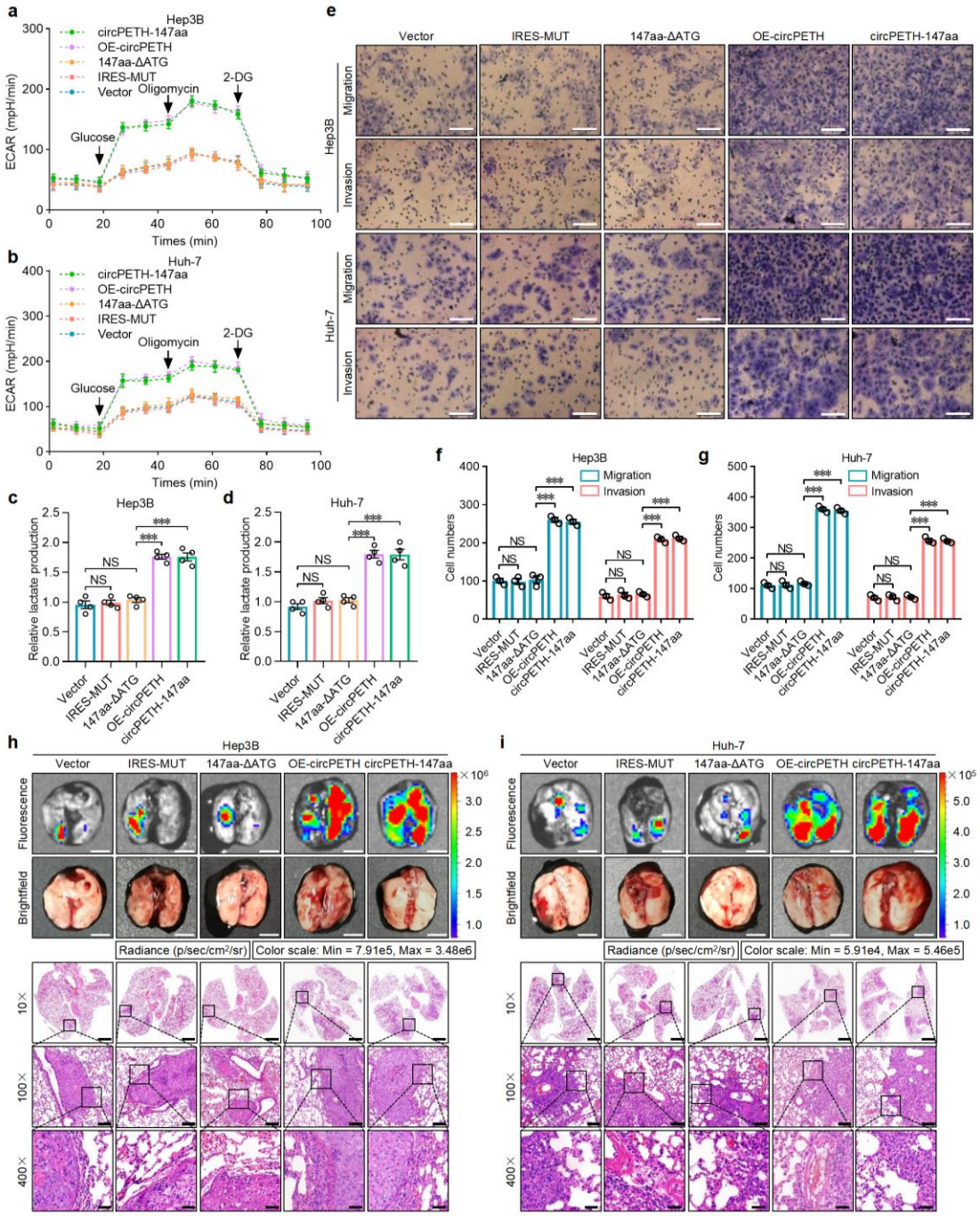


**a,b,** ECARs of Hep3B and Huh-7 cells transfected with five different vectors. **c,d,** Lactate production of Hep3B and Huh-7 cells transfected with five different vectors. $n = 4$ independent experiments. Data are shown as mean ± SEM. Exact *P* values from top to bottom (**c**): 9.01E−05, 1.64E−05. Exact *P* values from top to bottom (**d**): 0.000223, 5.22E−05. **e,** The invasion and migration of Hep3B and Huh-7 cells

transfected with five different vectors. Scale bar, 100 μm. **f,g,** Quantification of the invasion and migration of Hep3B and Huh-7 cells transfected with five different vectors. $n = 3$ independent experiments. Data are shown as mean ± SEM. Exact *P* values from top to bottom and left to right (**f**): 0.000156, 0.000138, 1.64E−05, 1.80E−05. Exact *P* values from top to bottom and left to right (**g**): 5.15E−06, 4.74E−06, 7.54E−06, 1.49E−05. **h,i,** Top: Representative fluorescence and brightfield photographs of pulmonary metastatic nodules in lung metastasis models with indicated Hep3B and Huh-7 cells. Bottom: Representative HE staining and statistical analysis of metastatic foci in the lung. Scale bars from top to bottom: 4 mm, 4 mm, 2.8 mm, 280 μm, 70 μm. $n = 5$ for each group. NS, not significant; ***, $P < 0.001$ by two-tailed Student's T-test. Data are representative of at least three independent experiments.

**Supplementary Fig. 9: Overexpression of circPETH-147aa or translatable circPETH promotes the metastasis of HCC cells, related to Fig. 2.**

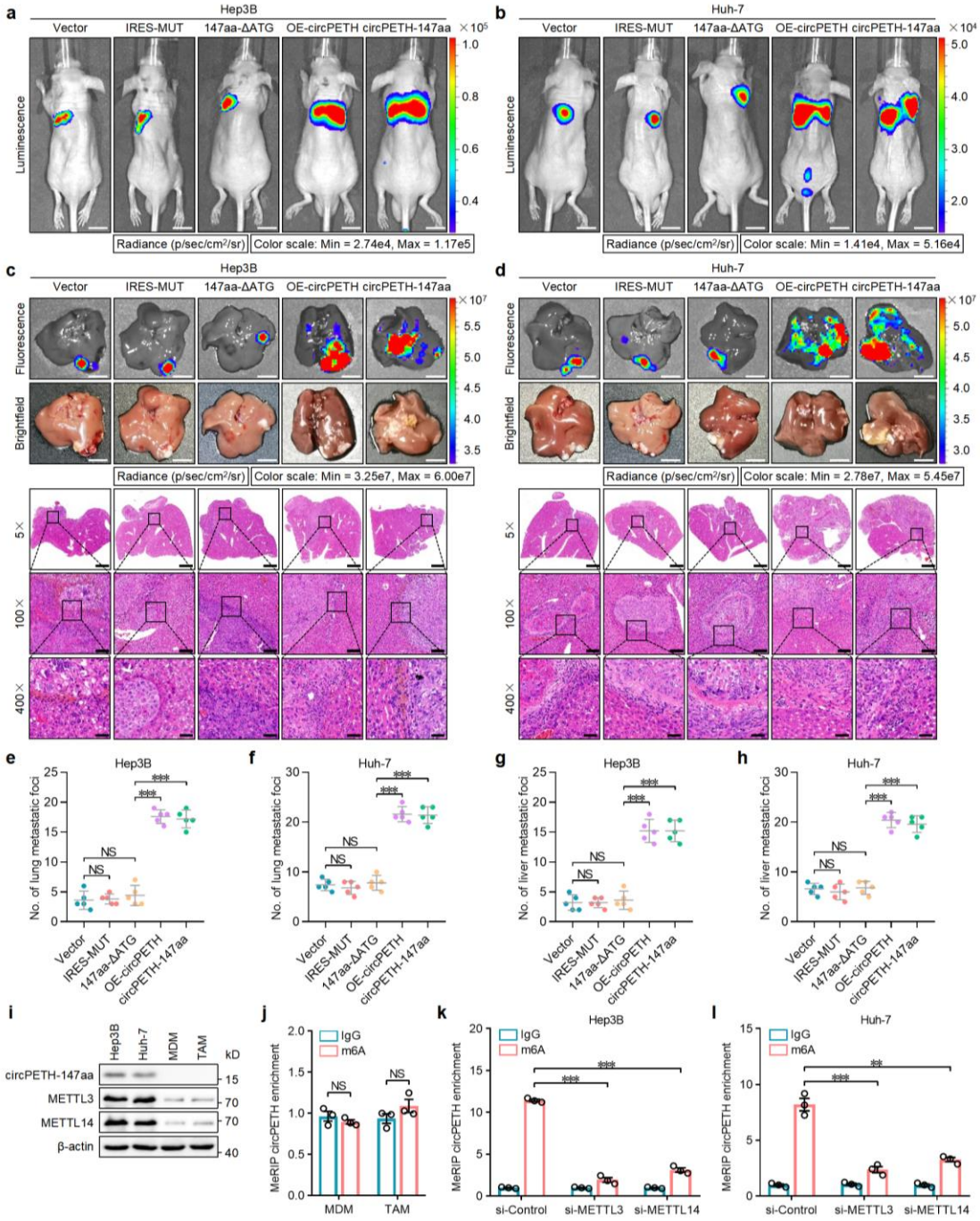


**a,b,** Representative bioluminescence photographs of the murine tail vein injection lung metastasis models with indicated Hep3B and Huh-7 cells. Scale bar, 1 cm. $n = 5$ for each group. **c,d,** Top: Representative fluorescence and brightfield photographs of intrahepatic metastatic nodules in liver orthotopic implanted intrahepatic metastasis models with indicated Hep3B and Huh-7 cells. Bottom: Representative HE staining of metastatic foci in the liver. Scale bars from top to bottom: 7.5 mm, 7.5 mm, 2.8 mm,

280 μm, 70 μm. $n = 5$ for each group. **e,f,** Statistical analysis of metastatic foci in the lung. $n = 5$ for each group. Data are shown as mean ± SD. Exact *P* values from top to bottom (**e**): 1.31E−06, 4.81E−07. Exact *P* values from top to bottom (**f**): 8.22E−07, 4.89E−07. **g,h,** Statistical analysis of metastatic foci in the liver. $n = 5$ for each group. Data are shown as mean ± SD. Exact *P* values from top to bottom (**g**): 3.98E−06, 5.53E−06. Exact *P* values from top to bottom (**h**): 8.73E−07, 3.47E−07. **i,** The expressions of circPETH-147aa, METTL3 and METTL14 in HCC cells and macrophages by western blot. The samples derive from the same experiment but different gels for circPETH-147aa, another for MTLL3, another for METTL14 and another for β-actin were processed in parallel. **j,** The m6A levels of circPETH in TAMs and MDMs by MeRIP assays. **k,l,** The m6A levels of circPETH in Hep3B and Huh-7 cells with knockdown of METTL3 or METTL14 by MeRIP assays. $n = 3$ independent experiments. Data are shown as mean ± SEM. Exact *P* values from top to bottom (**k**): 8.97E−06, 6.94E−06. Exact *P* values from top to bottom (**l**): 0.001116, 0.000702. NS, not significant; **, $P < 0.01$; ***, $P < 0.001$ by two-tailed Student's T-test. Data are representative of at least three independent experiments.

**Supplementary Fig. 10: m6A modification in IRES triggers a cap-independent protein translation from circPETH with the participation of EIF4G2 and YTHDF3, related to Fig. 2.**

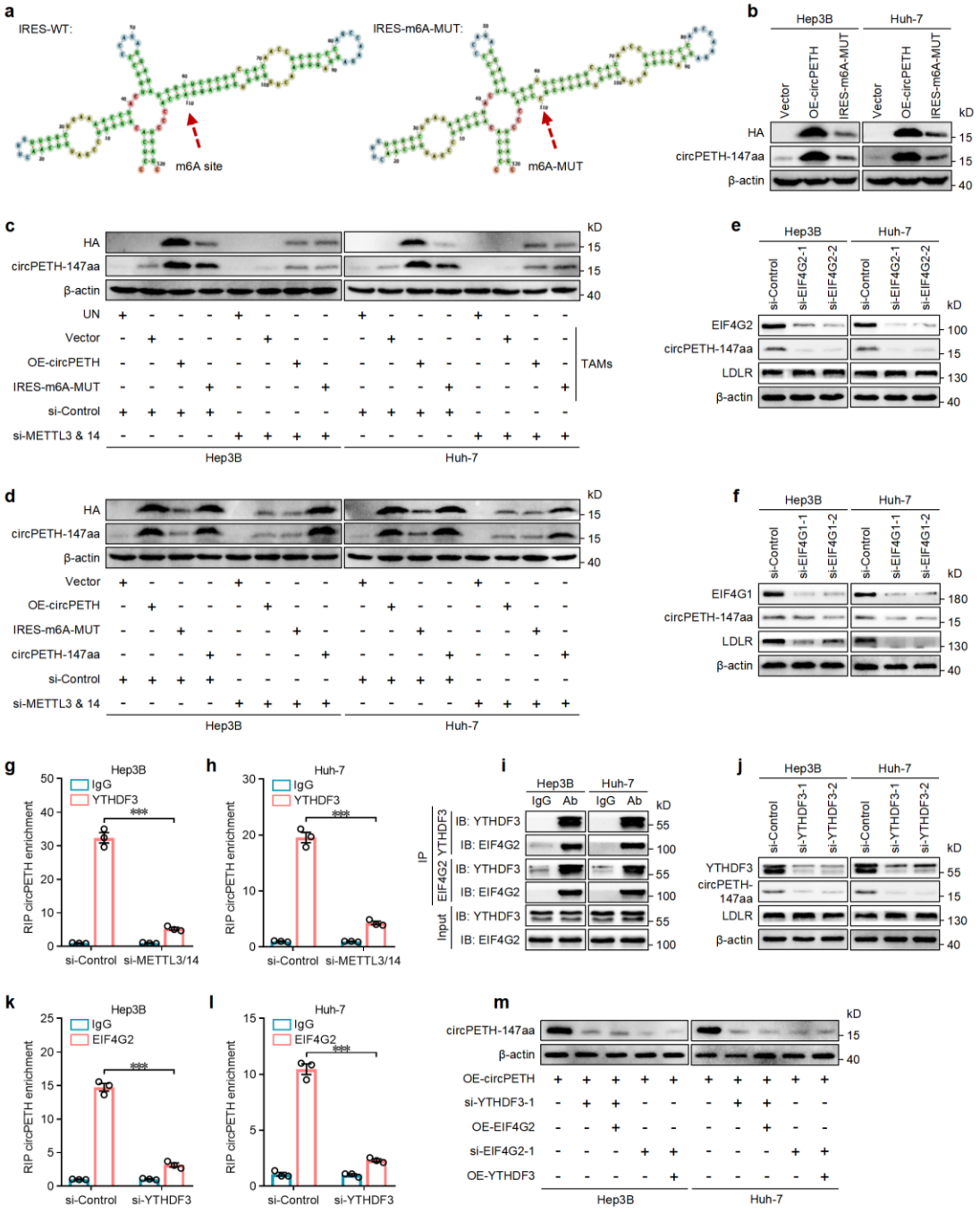


**a,** The predicted wild-type and m6A site-mutated secondary structures of IRES. **b,** The expressions of HA and circPETH-147aa in Hep3B and Huh-7 cells transfected with circPETH wild-type or IRES-m6A-MUT plasmid by western blot. The samples derive from the same experiment but different gels for circPETH-147aa, another for HA and another for β-actin were processed in parallel. **c,** The expressions of HA and circPETH-

147aa in Hep3B and Huh-7 cells cocultured with indicated TAMs and transfected with METTL3 and METTL14 siRNAs by western blot. The samples derive from the same experiment but different gels for circPETH-147aa, another for HA and another for β-actin were processed in parallel. **d,** The expressions of HA and circPETH-147aa in Hep3B and Huh-7 cells co-transfected with indicated plasmids and siRNAs targeting METTL3 and METTL14 by western blot. The samples derive from the same experiment but different gels for circPETH-147aa, another for HA and another for β-actin were processed in parallel. **e,** The expressions of EIF4G2, circPETH-147aa and LDLR in Hep3B and Huh-7 cells transfected with siRNAs targeting EIF4G2 by western blot. **f,** The expressions of EIF4G1, circPETH-147aa and LDLR in Hep3B and Huh-7 cells transfected with siRNAs targeting EIF4G1 by western blot. **g,h,** The enrichment of circPETH in YTHDF3-immunoprecipitated RNAs for Hep3B and Huh-7 cells transfected with siRNAs targeting METTL3 and METTL14 by RIP assays. $n = 3$ independent experiments. Data are shown as mean ± SEM. Exact *P* value (**g**): 7.17E−05. Exact *P* value (**h**): 0.000101. **i,** The interaction between YTHDF3 and EIF4G2 by reciprocal co-IP assays. **j,** The expressions of YTHDF3, circPETH-147aa and LDLR in Hep3B and Huh-7 cells transfected with siRNAs targeting YTHDF3 by western blot. **k,l,** The enrichment of circPETH in EIF4G2-immunoprecipitated RNAs for Hep3B and Huh-7 cells transfected with siRNAs targeting YTHDF3 by RIP assays. $n = 3$ independent experiments. Data are shown as mean ± SEM. Exact *P* value (**k**): 5.83E−05. Exact *P* value (**l**): 7.71E−05. **m,** circPETH-147aa expression in indicated Hep3B and Huh-7 cells by western blot. The samples derive from the same experiment but different gels for circPETH-147aa, and another for β-actin were processed in parallel. ***, $P < 0.001$ by two-tailed Student's T-test. Data are representative of at least three independent experiments.

**Supplementary Fig. 11: circPETH modulates the cytoskeletal reorganization and Hippo signaling pathway in HCC cells, related to Fig. 2.**

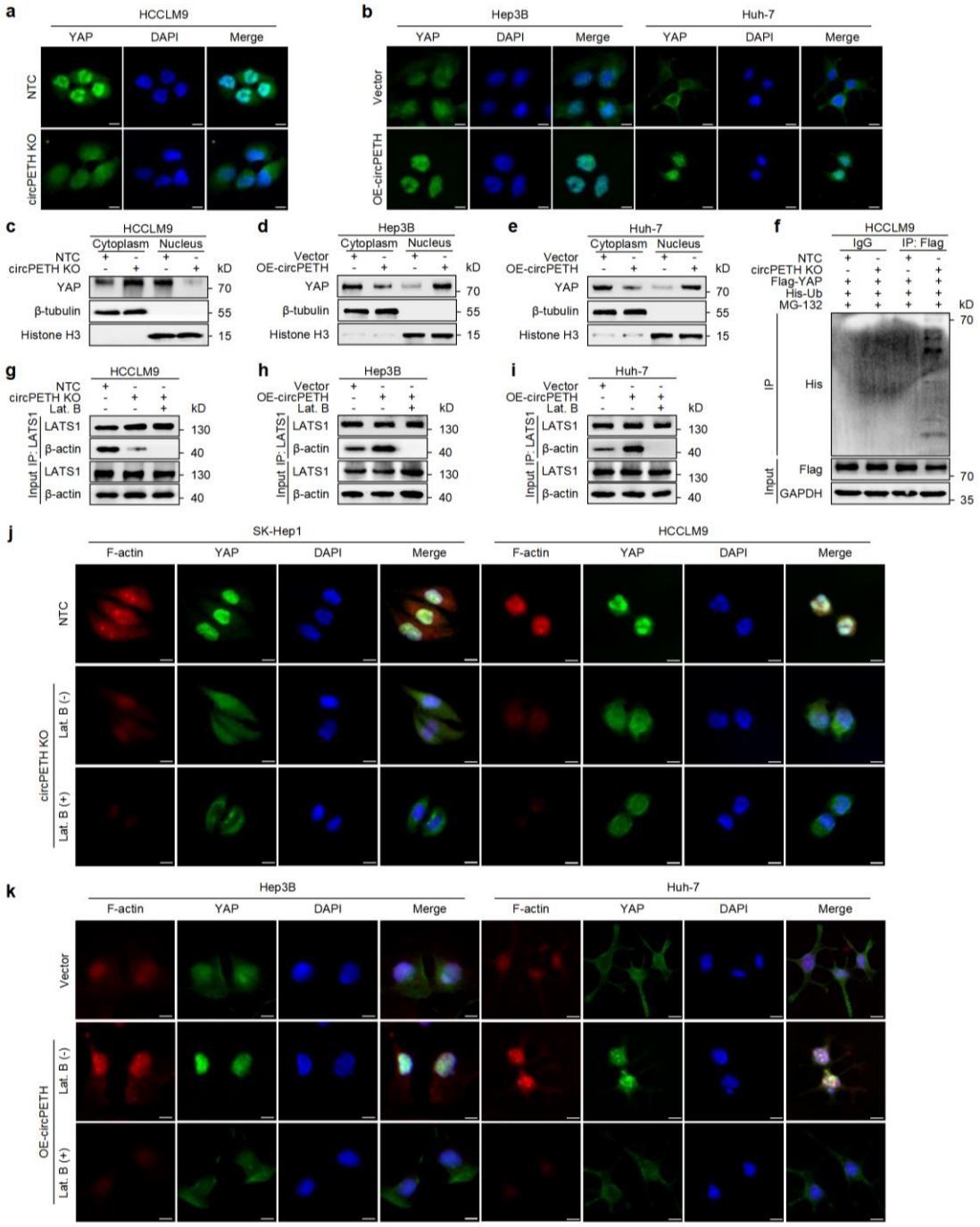


**a,** Subcellular location of YAP in HCCLM9 cells with circPETH KO by IF. Scale bar, 10 μm. **b,** Subcellular location of YAP in Hep3B and Huh-7 cells with circPETH overexpression by IF. Scale bar, 10 μm. **c,** Subcellular location of YAP in HCCLM9 cells with circPETH KO by subcellular protein fractionation. **d,e,** Subcellular location of YAP in Hep3B and Huh-7 cells with circPETH overexpression by subcellular protein fractionation. **f,** His-tagged ubiquitin and Flag-tagged YAP were simultaneously

overexpressed in HCC cells to evaluate the effect of circPETH on YAP ubiquitination. Cells were treated with 25 μM MG132 for 4 hours before harvest to avoid degradation of ubiquitinated proteins. The samples derive from the same experiment but different gels for His, another for Flag and GAPDH were processed in parallel. **g-i,** The interaction between LATS1 and F-actin was determined by co-IP assays. **j,k,** Cells were treated with 1 μg/mL Lat. B for 1 hour to disrupt the cytoskeleton prior to IF. Scale bar, 10 μm. Data are representative of at least three independent experiments.

**Supplementary Fig. 12: circPETH modulates the cytoskeletal reorganization and multiple signaling pathway in HCC cells, related to Fig. 2.**

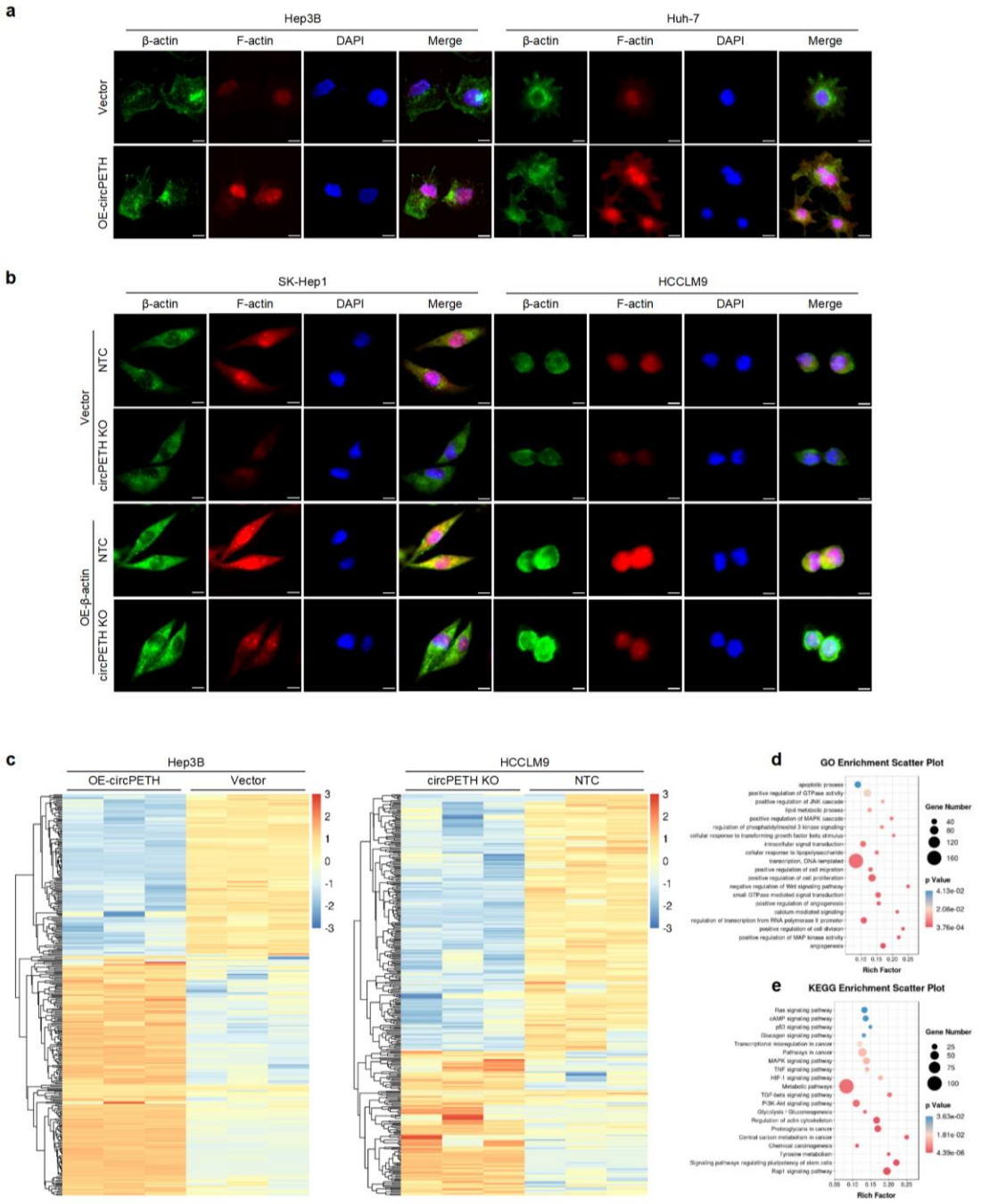


**a,b,** The expressions of β-actin and F-actin upon circPETH overexpression and knockout were determined by IF. Scale bar, 10 μm. **c,** Heatmap of differentially expressed genes upon circPETH overexpression and knockout by RNA-seq. **d,e,** GO and KEGG analysis of the differentially expressed genes. Data are representative of at least three independent experiments.

**Supplementary Fig. 13: circPETH-147aa consolidates the interaction between PKM2 and ALDOA by simultaneously binding to PKM2 and ALDOA, related to Fig. 3.**

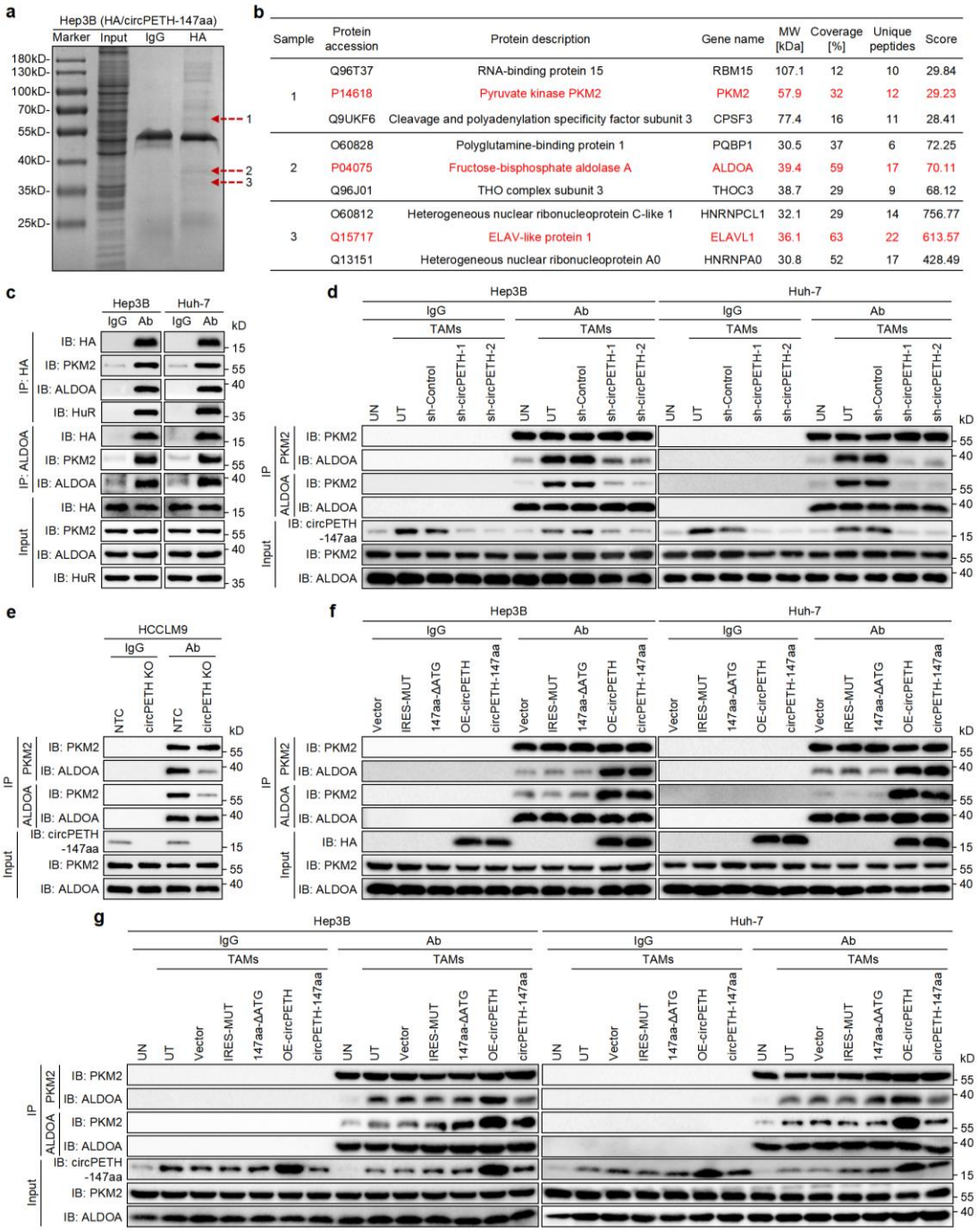


**a,** Total proteins were extracted from Hep3B cells transfected with HA-tagged circPETH-147aa coimmunoprecipitated with antibody against HA and separated through SDS-PAGE, followed by Coomassie brilliant blue staining. The specific bands of interest (shown as red arrows) were subjected to MS. **b,** The Supplementary Table

hows MS results identifying the possible binding proteins. **c,** The interaction among circPETH-147aa, PKM2 and ALDOA, and the mutual interaction between circPETH-147aa and HuR were by co-IP assays. The samples derive from the same experiment but different gels for HA and PKM2, another for HuR, ALDOA and HA, another for PKM2, ALDOA and HA, another for PKM2 and ALDO1 and another for HuR were processed in parallel. **d,** The interaction between PKM2 and ALDOA in Hep3B and Huh-7 cells cocultured with indicated TAMs by co-IP assays. The samples derive from the same experiment but different gels for PKM2 and ALDOA, another for PKM2, ALDOA and circPETH-147aa, and another for PKM2 and ALDOA were processed in parallel. **e,** The interaction between PKM2 and ALDOA in HCCLM9 cells with circPETH KO by co-IP assays. The samples derive from the same experiment but different gels for PKM2 and ALDOA, another for PKM2, ALDOA and circPETH-147aa, and another for PKM2 and ALDOA were processed in parallel. **f,** The interaction between PKM2 and ALDOA in indicated Hep3B and Huh-7 cells by co-IP assays. The samples derive from the same experiment but different gels for PKM2 and ALDOA, another for PKM2, ALDOA and HA, and another for PKM2 and ALDOA were processed in parallel. **g,** The interaction between PKM2 and ALDOA in Hep3B and Huh-7 cells cocultured with indicated TAMs by co-IP assays. The samples derive from the same experiment but different gels for PKM2 and ALDOA, another for PKM2, ALDOA and circPETH-147aa, and another for PKM2 and ALDOA were processed in parallel. Data are representative of at least three independent experiments.

**Supplementary Fig. 14: circPETH-147aa functions as a guide that enhances the phosphorylation of ALDOA catalyzed by PKM2, related to Fig. 3.**

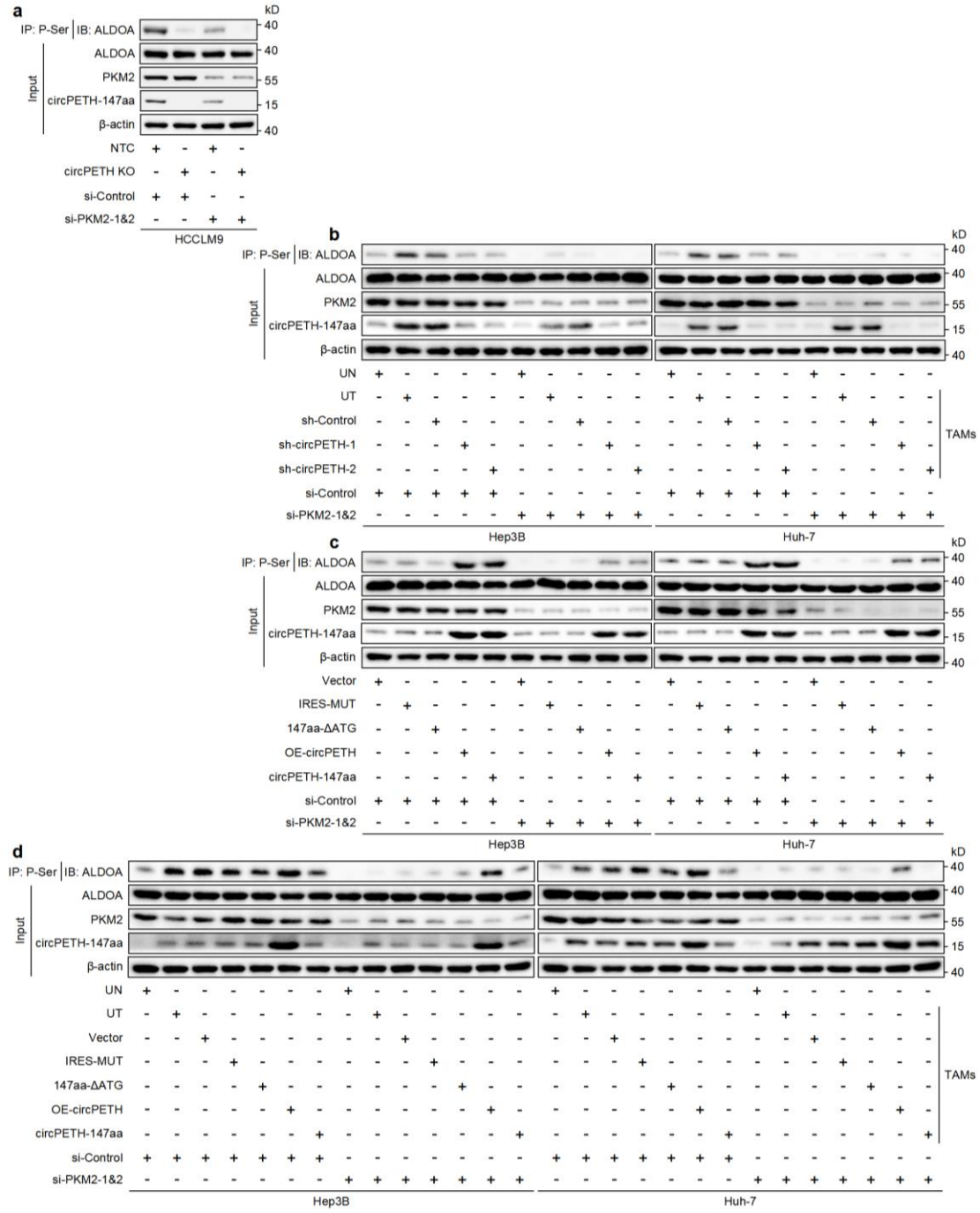


**a,** The phosphorylation level of ALDOA in HCCLM9 cells with circPETH KO and PKM2 knockdown by co-IP assays. The samples derive from the same experiment but different gels for β-actin and ALDOA, another for PKM2, ALDOA and circPETH-147aa, and another for PKM2 and ALDOA were processed in parallel. **b,** The phosphorylation level of ALDOA in Hep3B and Huh-7 cells cocultured with indicated TAMs and transfected with siRNAs targeting PKM2 by co-IP assays. The samples

derive from the same experiment but different gels for β-actin and ALDOA, another for PKM2, ALDOA and circPETH-147aa, and another for PKM2 and ALDOA were processed in parallel. **c,** The phosphorylation level of ALDOA in indicated Hep3B and Huh-7 cells with PKM2 knockdown by co-IP assays. The samples derive from the same experiment but different gels for β-actin and ALDOA, another for PKM2, ALDOA and circPETH-147aa, and another for PKM2 and ALDOA were processed in parallel. **d,** The phosphorylation level of ALDOA in Hep3B and Huh-7 cells cocultured with indicated TAMs and transfected with siRNAs targeting PKM2 by co-IP assays. The samples derive from the same experiment but different gels for β-actin and ALDOA, another for PKM2, ALDOA and circPETH-147aa, and another for PKM2 and ALDOA were processed in parallel. Data are representative of at least three independent experiments.

**Supplementary Fig. 15: ALDOA binds to PKM2 via a hydrophobic pocket, related to Fig. 3.**

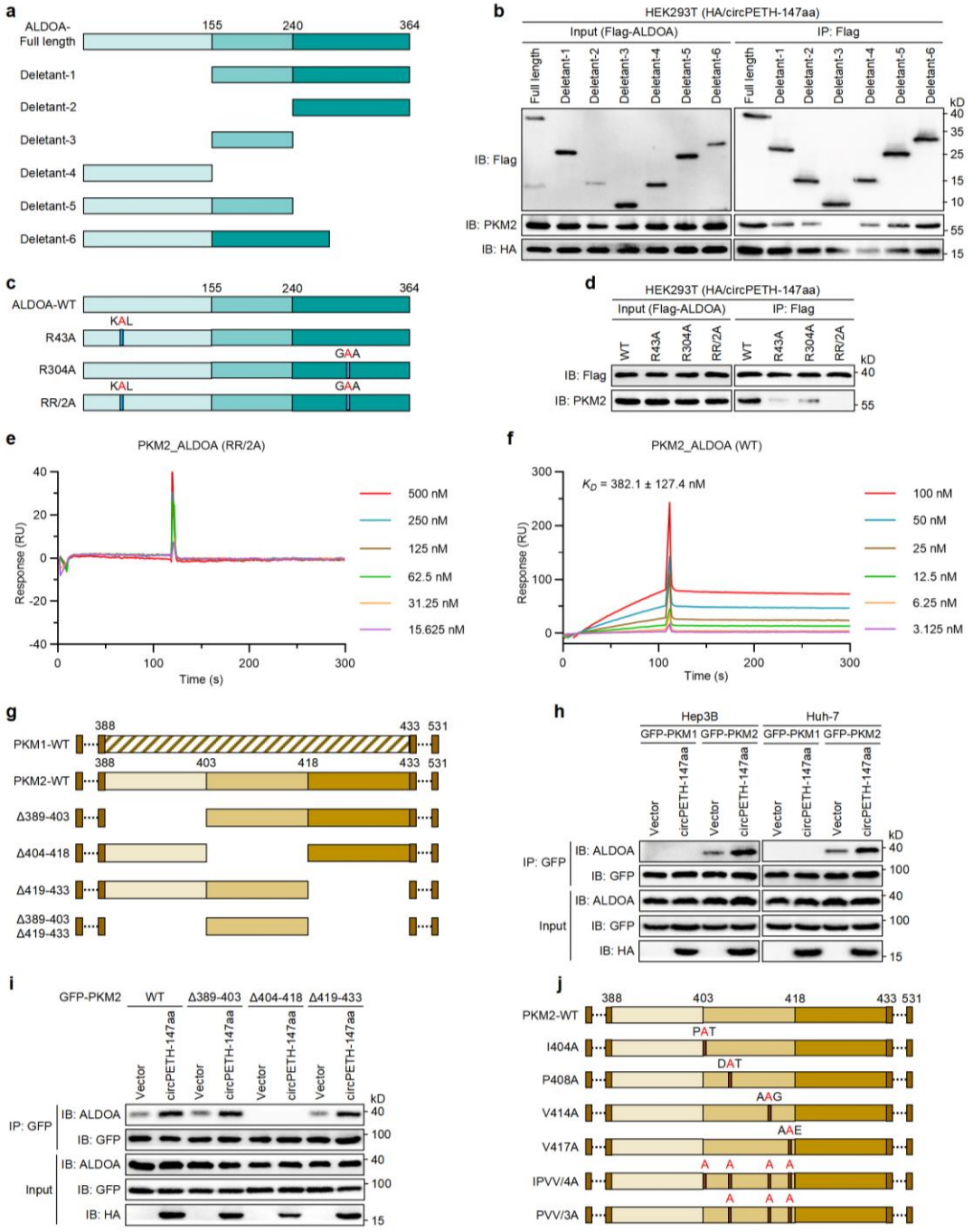


**a,** Schematic of Flag-tagged ALDOA deletion mutants. **b,** HEK293T cells were transfected with HA-tagged circPETH-147aa and Flag-tagged full-length or ALDOA fragments, followed by co-IP assays. **c,** Schematic of Flag-tagged ALDOA site-directed mutants. **d,** HEK293T cells were transfected with HA-tagged circPETH-147aa and Flag-tagged ALDOA site-directed mutants, followed by co-IP assays. **e,** SPR sensorgrams and binding affinity between site-mutated ALDOA and PKM2. **f,** SPR

sensorgrams and binding affinity between wild-type ALDOA and PKM2. **g,** Schematic of GFP-tagged PKM1 and GFP-tagged PKM2 deletion mutants. **h,** The interaction of ALDOA and GFP-tagged PKM1 or GFP-tagged PKM2 in Hep3B and Huh-7 cells with circPETH-147aa overexpression by co-IP assays. The samples derive from the same experiment but different gels for GFP and ALDOA, and another for GFP, ALDOA and HA were processed in parallel. **i,** The interactions of ALDOA and GFP-tagged PKM2 deletion mutants in HEK293T cells with circPETH-147aa overexpression by co-IP assays. The samples derive from the same experiment but different gels for GFP and ALDOA, and another for GFP, ALDOA and HA were processed in parallel. **j,** Schematic of GFP-tagged PKM2 site-directed mutants. Data are representative of at least three independent experiments.

**Supplementary Fig. 16: PKM2 binds to ALDOA via I404 residue, related to Fig. 3.**

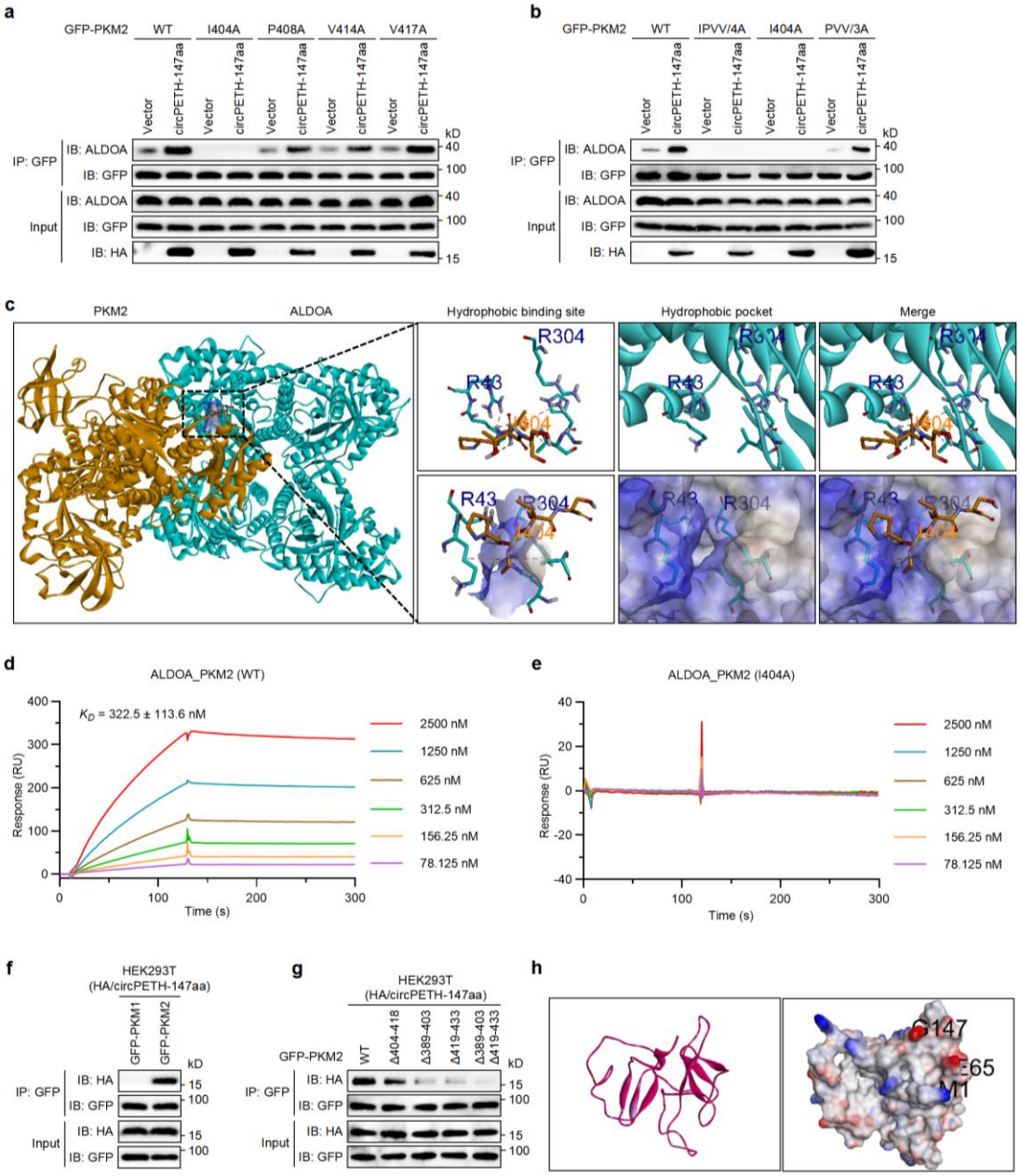


**a,b,** The interactions of ALDOA and GFP-tagged PKM2 site-directed mutants in HEK293T cells with circPETH-147aa overexpression by co-IP assays. The samples derive from the same experiment but different gels for GFP and ALDOA, and another for GFP, ALDOA and HA were processed in parallel. **c,** Molecular docking of 3-dimensional structures shows the interaction of the I404 residue of PKM2 with the hydrophobic pocket of ALDOA. **d,** SPR sensorgrams and binding affinity between wild-type PKM2 and ALDOA. **e,** SPR sensorgrams and binding affinity between site-

mutated PKM2 and ALDOA. **f,** The interaction of HA-tagged circPETH-147aa and GFP-tagged PKM1 or GFP-tagged PKM2 in HEK293T cells by co-IP assays. The samples derive from the same experiment but different gels for GFP and HA, and another for GFP and HA were processed in parallel. **g,** The interactions of HA-tagged circPETH-147aa and GFP-tagged PKM2 deletion mutants in HEK293T cells by co-IP assays. The samples derive from the same experiment but different gels for GFP and HA, and another for GFP and HA were processed in parallel. **h,** The predicted 3-dimensional structure of circPETH-147aa. Data are representative of at least three independent experiments.

**Supplementary Fig. 17: The P96 and P106 residues of circPETH-147aa respectively interact with two pockets of PKM2, related to Fig. 3.**

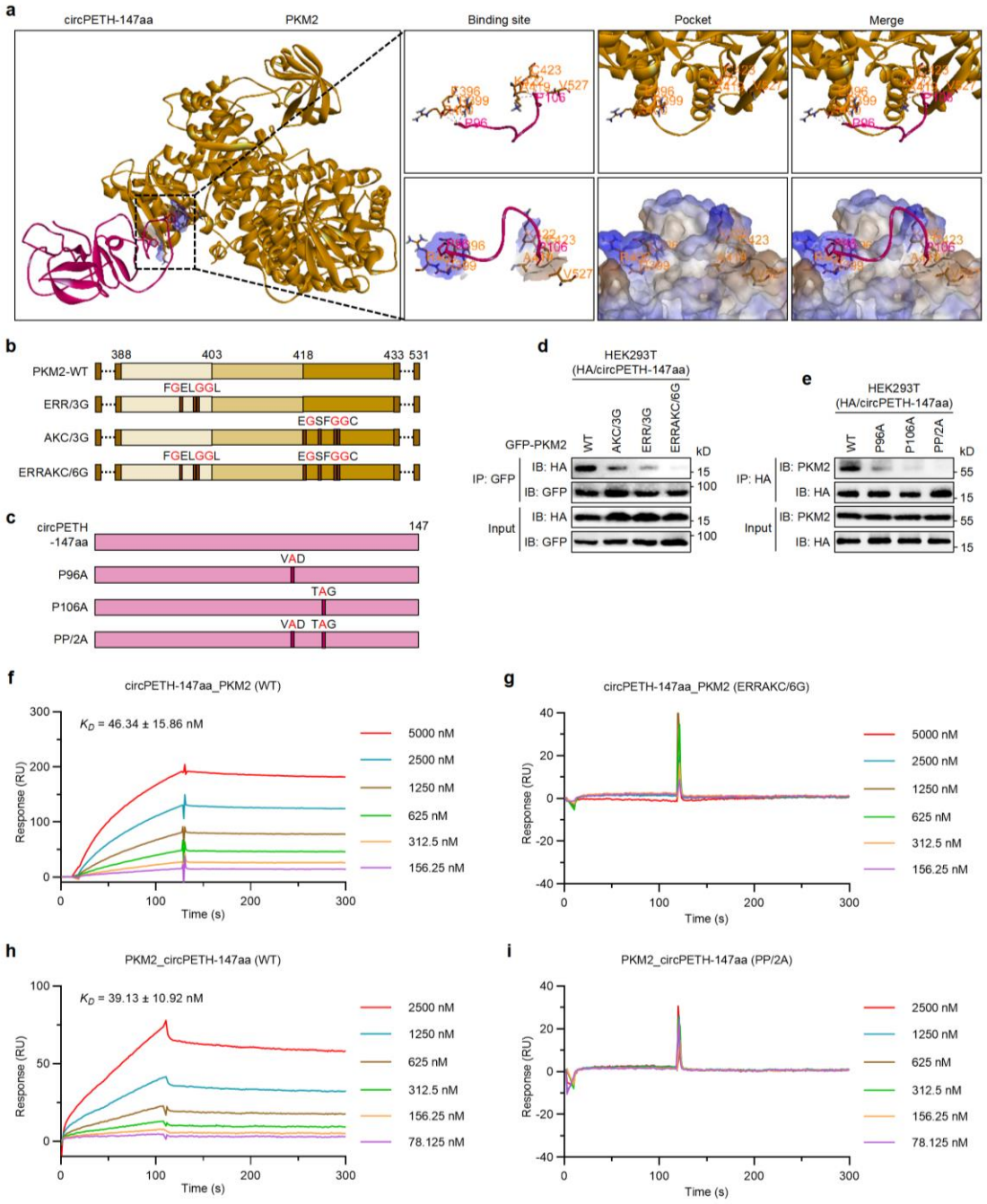


**a,** Molecular docking of 3-dimensional structures shows the interactions of the P96 and P106 residues of circPETH-147aa with two pockets of PKM2. **b,** Schematic of GFP-tagged PKM2 site-directed mutants. **c,** Schematic of HA-tagged circPETH-147aa site-directed mutants. **d,** The interactions of HA-tagged circPETH-147aa and GFP-tagged PKM2 site-directed mutants in HEK293T cells by co-IP assays. The samples derive from the same experiment but different gels for GFP and HA, and another for GFP and

HA were processed in parallel. **e,** The interactions of PKM2 and HA-tagged circPETH-147aa site-directed mutants in HEK293T cells by co-IP assays. The samples derive from the same experiment but different gels for PKM2 and HA, and another for PKM2 and HA were processed in parallel. **f,** SPR sensorgrams and binding affinity between wild-type PKM2 and circPETH-147aa. **g,** SPR sensorgrams and binding affinity between site-mutated PKM2 and circPETH-147aa. **h,** SPR sensorgrams and binding affinity between wild-type circPETH-147aa and PKM2. **i,** SPR sensorgrams and binding affinity between site-mutated circPETH-147aa and PKM2. Data are representative of at least three independent experiments.

**Supplementary Fig. 18: Three sets of amino acids residues of ALDOA fit into the MEG pocket of circPETH-147aa, related to Fig. 3.**

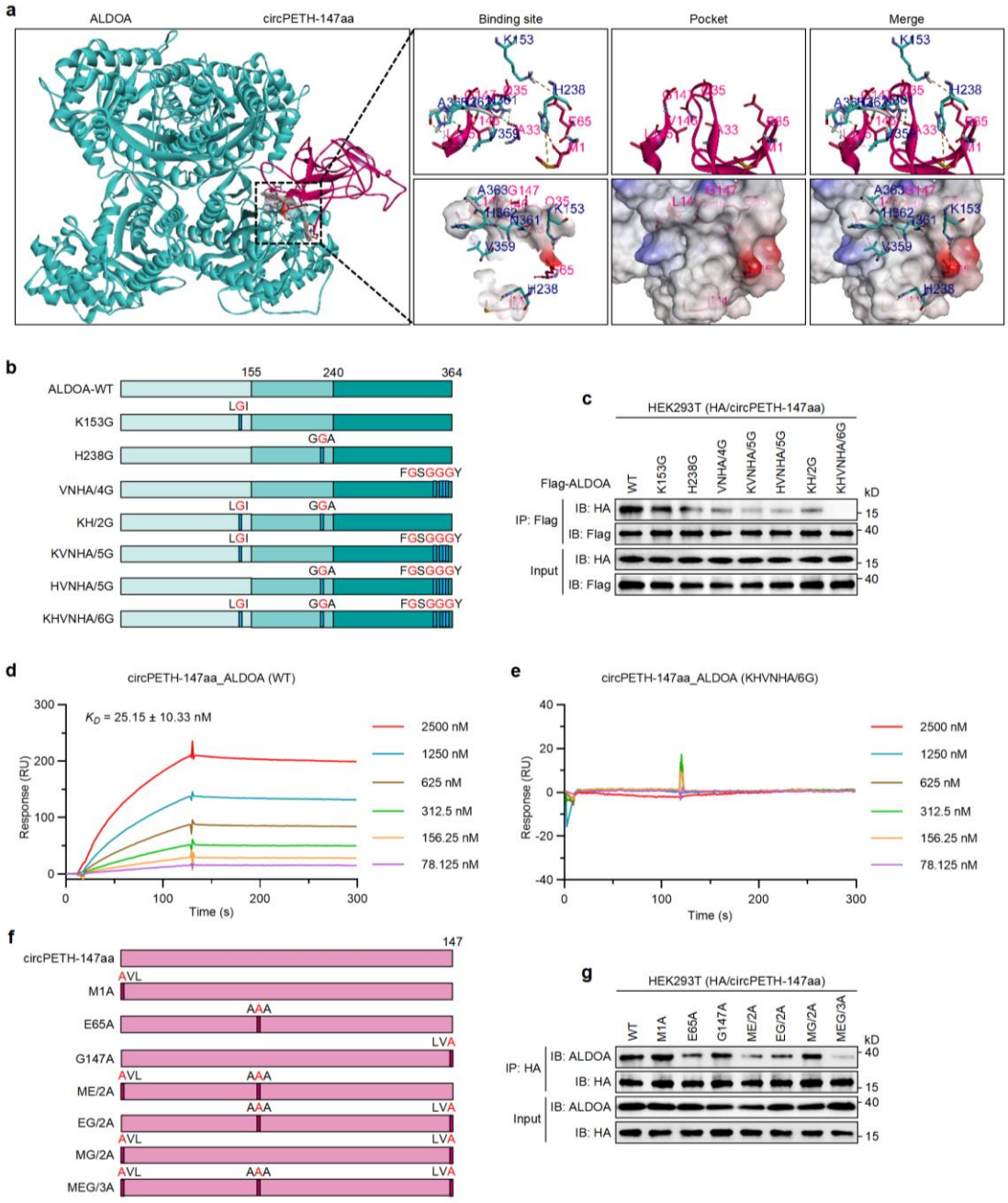


**a,** Molecular docking of 3-dimensional structures shows the interaction of three sets of amino acids residues of ALDOA with the MEG pocket of circPETH-147aa. **b,** Schematic of Flag-tagged ALDOA site-directed mutants. **c,** The interactions of HA-tagged circPETH-147aa and Flag-tagged ALDOA site-directed mutants in HEK293T cells by co-IP assays. The samples derive from the same experiment but different gels for Flag and HA, and another for Flag and HA were processed in parallel. **d,** SPR

sensorgrams and binding affinity between wild-type ALDOA and circPETH-147aa. **e,** SPR sensorgrams and binding affinity between site-mutated ALDOA and circPETH-147aa. **f,** Schematic of HA-tagged circPETH-147aa site-directed mutants. **g,** The interactions of ALDOA and HA-tagged circPETH-147aa site-directed mutants in HEK293T cells by co-IP assays. The samples derive from the same experiment but different gels for ALDOA and HA, and another for ALDOA and HA were processed in parallel. Data are representative of at least three independent experiments.

**Supplementary Fig. 19: MEG pocket mediates the biological functions of circPETH-147aa, related to Fig. 3.**

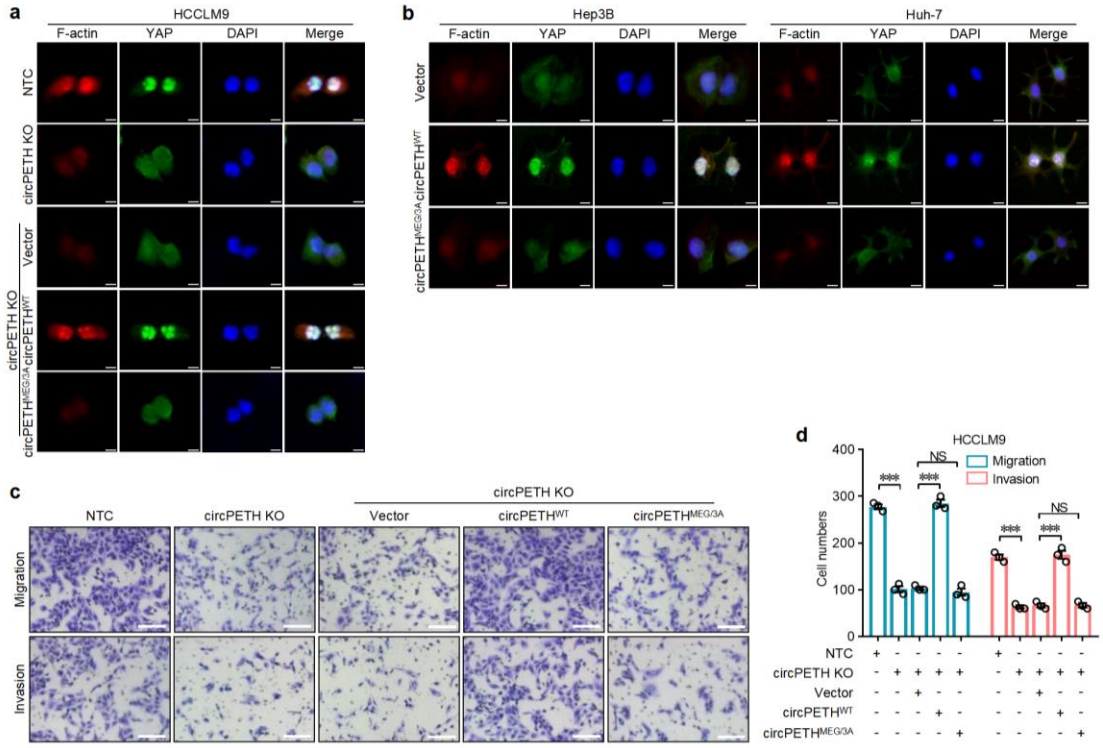


**a,** Subcellular location of YAP in HCCLM9 cells with circPETH KO and overexpression of wild-type or MEG/3A mutated circPETH-147aa by IF. Scale bar, 10 μm. **b,** Subcellular location of YAP in Hep3B and Huh-7 cells with overexpression of wild-type or MEG/3A mutated circPETH-147aa by IF. Scale bar, 10 μm. **c,** The invasion and migration of HCCLM9 cells with circPETH KO and overexpression of wild-type or MEG/3A mutated circPETH-147aa. Scale bar, 100 μm. **d,** Quantification of the invasion and migration of HCCLM9 cells with circPETH KO and overexpression of wild-type or MEG/3A mutated circPETH-147aa. $n = 3$ independent experiments. Data are shown as mean ± SEM. Exact $P$ values from left to right: 2.87E−05, 2.62E−05, 8.92E−05, 0.000369. NS, not significant; ***, $P < 0.001$ by two-tailed Student's T-test. Data are representative of at least three independent experiments.

**Supplementary Fig. 20: circPETH-147aa increases the binding of HuR to SLC43A2 mRNA, related to Fig. 4.**

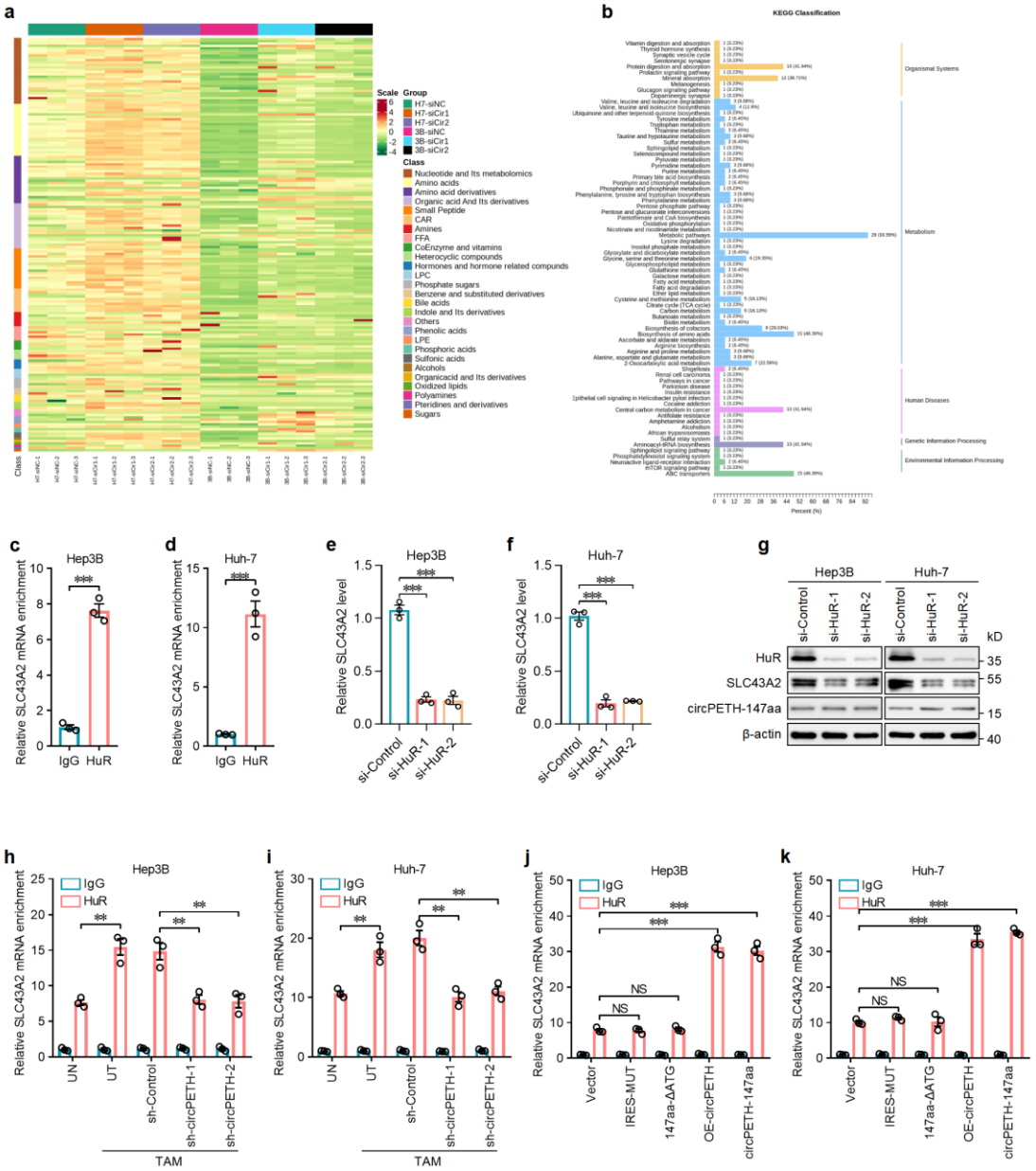


**a,** Heatmap of metabolomics for Hep3B and Huh-7 cells with circPETH knockdown. **b,** KEGG analysis of the metabolites with different contents in metabolomics. **c,d,** The enrichment of SLC43A2 mRNA in HuR-immunoprecipitated RNAs for Hep3B and Huh-7 cells by RIP assays. $n = 3$ independent experiments. Data are shown as mean ± SEM. Exact *P* value (**c**): 7.59E−05. Exact *P* value (**d**): 0.000716. **e,f,** SLC43A2 expression in Hep3B and Huh-7 cells transfected with siRNAs targeting HuR by qRT-

PCR. $n = 3$ independent experiments. Data are shown as mean ± SEM. Exact *P* values from top to bottom (**e**): 0.000132, 8.19E−05. Exact *P* values from top to bottom (**f**): 3.75E−05, 9.36E−05. **g,** The expressions of HuR, SLC43A2 and circPETH-147aa in Hep3B and Huh-7 cells transfected with siRNAs targeting HuR by western blot. **h,i,** The enrichment of SLC43A2 mRNA in HuR-immunoprecipitated RNAs for Hep3B and Huh-7 cells cocultured with indicated TAMs by RIP assays. $n = 3$ independent experiments. Data are shown as mean ± SEM. Exact *P* values from left to right and top to bottom (**h**): 0.002868, 0.008918, 0.006910. Exact *P* values from left to right and top to bottom (**i**): 0.005592, 0.003887, 0.002919. **j,k,** The enrichment of SLC43A2 mRNA in HuR-immunoprecipitated RNAs for indicated Hep3B and Huh-7 cells by RIP assays. $n = 3$ independent experiments. Data are shown as mean ± SEM. Exact *P* values from top to bottom (**j**): 7.39E−05, 8.42E−05. Exact *P* values from top to bottom (**k**): 3.08E−06, 0.000114. NS, not significant; **, $P < 0.01$; ***, $P < 0.001$ by two-tailed Student's T-test. Data are representative of at least three independent experiments.

**Supplementary Fig. 21: circPETH-147aa elevates the HuR-mediated expression of SLC43A2, related to Fig. 4.**

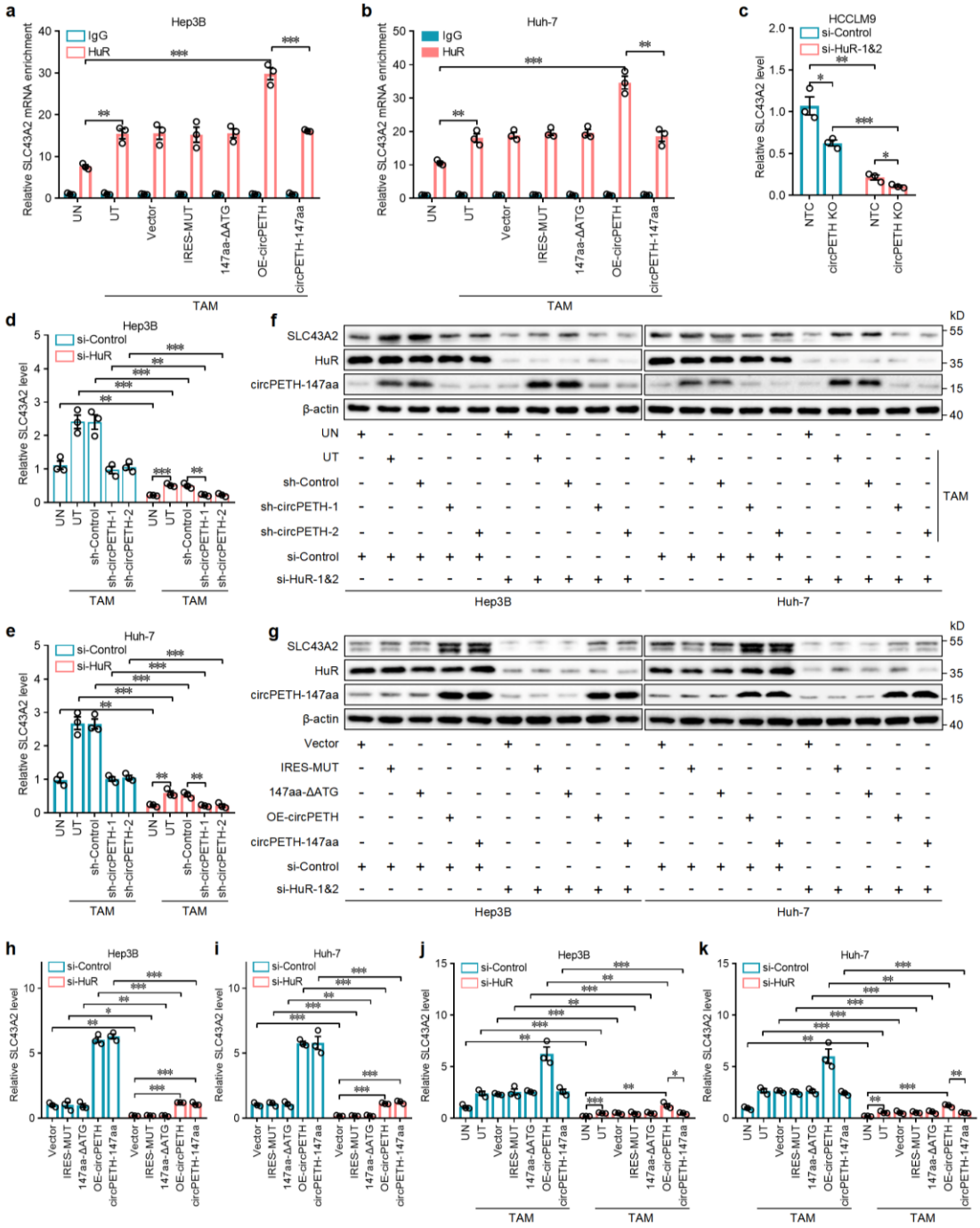


**a,b,** The enrichment of SLC43A2 mRNA in HuR-immunoprecipitated RNAs for Hep3B and Huh-7 cells cocultured with indicated TAMs by RIP assays. $n = 3$ independent experiments. Data are shown as mean ± SEM. Exact *P* values from top to bottom (**a**): 0.000716, 0.000120, 0.002868. Exact *P* values from top to bottom (**b**): 0.002823, 0.000273, 0.005592. **c,** SLC43A2 expression in HCCLM9 cells with circPETH KO and HuR knockdown by qRT-PCR. $n = 3$ independent experiments. Data

are shown as mean ± SEM. Exact *P* values from top to bottom: 0.001526, 0.016828, 0.000157, 0.030166. **d,e,** SLC43A2 expression in Hep3B and Huh-7 cells with indicated TAMs coculture and HuR knockdown by qRT-PCR. $n = 3$ independent experiments. Data are shown as mean ± SEM. Exact *P* values from top to bottom and left to right (**d**): 0.000770, 0.001879, 0.000999, 0.000749, 0.002091, 0.000451, 0.004293. Exact *P* values from top to bottom and left to right (**e**): 0.000404, 0.000218, 0.000159, 0.000498, 0.001113, 0.005833, 0.003475. **f,** The expressions of SLC43A2, HuR and circPETH-147aa in Hep3B and Huh-7 cells with indicated TAMs coculture and HuR knockdown by western blot. The samples derive from the same experiment but different gels for SLC43A2, and another for β-actin, HuR and circPETH-147aa were processed in parallel. **g,** The expressions of SLC43A2, HuR and circPETH-147aa in indicated Hep3B and Huh-7 cells with HuR knockdown by western blot. The samples derive from the same experiment but different gels for SLC43A2, and another for β-actin, HuR and circPETH-147aa were processed in parallel. **h,i,** SLC43A2 expression in indicated Hep3B and Huh-7 cells with HuR knockdown by qRT-PCR. $n = 3$ independent experiments. Data are shown as mean ± SEM. Exact *P* values from top to bottom (**h**): 1.09E−05, 2.26E−05, 0.007515, 0.021595, 0.001545, 0.000301, 1.66E−06. Exact *P* values from top to bottom (**i**): 0.000935, 4.97E−06, 0.002061, 0.000552, 0.000610, 0.000113, 1.46E−05. **j,k,** The expressions of SLC43A2, HuR and circPETH-147aa in Hep3B and Huh-7 cells with indicated TAMs coculture and HuR knockdown by qRT-PCR. $n = 3$ independent experiments. Data are shown as mean ± SEM. Exact *P* values from top to bottom (**j**): 0.000769, 0.001709, 1.52E−05, 0.002428, 1.38E−05, 0.000749, 0.002091, 0.014054, 0.003794, 0.000451. Exact *P* values from top to bottom (**k**): 9.50E−05, 0.002370, 0.000314, 5.35E−05, 7.61E−05, 0.000498, 0.001113, 0.001494, 0.000319, 0.005833. *, $P < 0.05$; **, $P < 0.01$; ***, $P < 0.001$ by two-tailed Student's T-test. Data are representative of at least three independent experiments.

**Supplementary Fig. 22: circPETH-147aa stimulates methionine and leucine consumption in HCC cells by elevating HuR-dependent SLC43A2 mRNA stability, related to Fig. 4.**

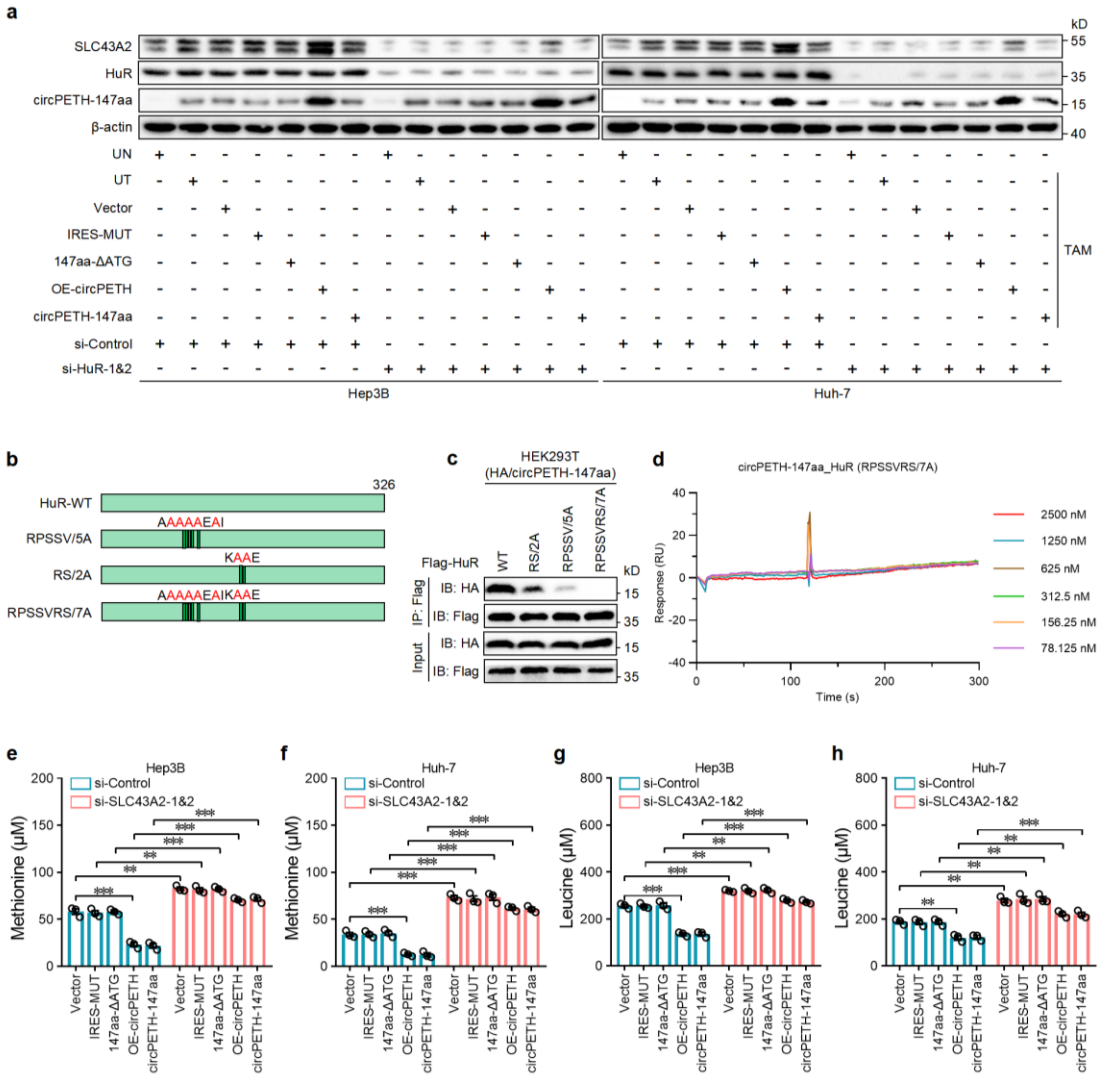


**a,** The expressions of SLC43A2, HuR and circPETH-147aa in Hep3B and Huh-7 cells with indicated TAMs coculture and HuR knockdown by western blot. The samples derive from the same experiment but different gels for SLC43A2, and another for β-actin, HuR and circPETH-147aa were processed in parallel. **b,** Schematic of Flag-tagged HuR site-directed mutants. **c,** The interactions of HA-tagged circPETH-147aa

and Flag-tagged HuR site-directed mutants in HEK293T cells by co-IP assays. The samples derive from the same experiment but different gels for Flag and HA, and another for Flag and HA were processed in parallel. **d,** SPR sensorgrams and binding affinity between site-mutated HuR and circPETH-147aa. **e-h,** Effects of indicated Hep3B and Huh-7 cells on methionine and leucine consumption for 24 h. $n = 3$ independent experiments. Data are shown as mean ± SEM. Exact *P* values from top to bottom (**e**): 7.14E−05, 3.69E−05, 0.000405, 0.001490, 0.001763, 0.000522. Exact *P* values from top to bottom (**f**): 4.90E−05, 1.26E−05, 0.000546, 0.000452, 0.000172, 0.000737. Exact *P* values from top to bottom (**g**): 8.57E−05, 4.07E−05, 0.005447, 0.002205, 0.000722, 0.000129. Exact *P* values from top to bottom (**h**): 0.000950, 0.001178, 0.001602, 0.002370, 0.001176, 0.003974. **, $P < 0.01$; ***, $P < 0.001$ by two-tailed Student's T-test. Data are representative of at least three independent experiments.

**Supplementary Fig. 23: circPETH-147aa impairs anti-HCC immunity by inducing methionine and leucine deficiency in cytotoxic CD8$^+$ T cells, related to Fig. 4.**

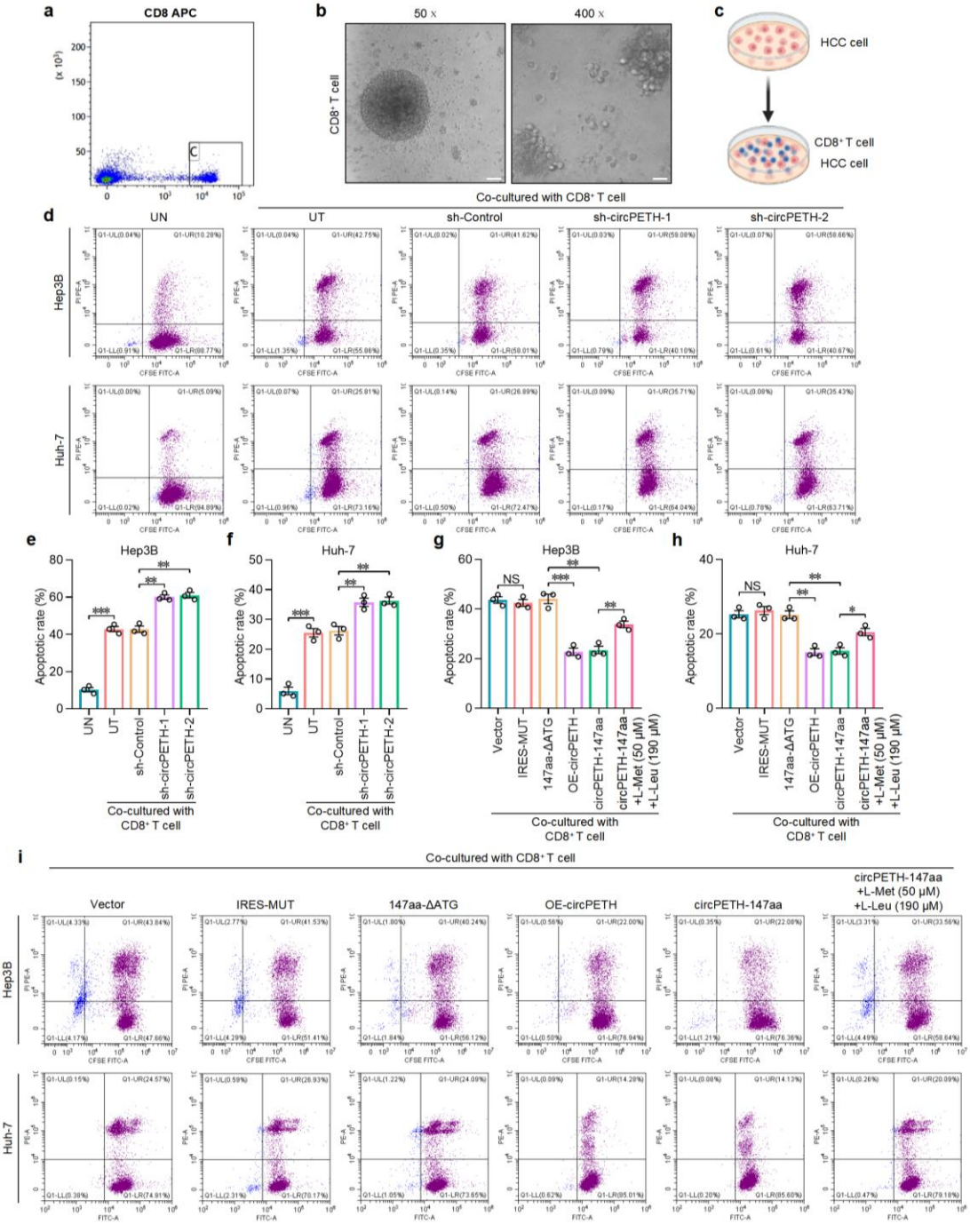


**a,** FACS of CD8$^+$ T cells isolated from human peripheral blood. **b,** Phase-contrast micrographs of activated and amplified CD8$^+$ T cells by IL-2, anti-CD3 and anti-CD28 antibodies with different magnifications. Scale bars from left to right: 50 μm, 6.25μm. **c,** Schematic of HCC cells directly cocultured with CD8$^+$ T cells [Created in BioRender.

Cai, Y. (2024) https://BioRender.com/v84x844]. **d,** Flow cytometry analysis of indicated Hep3B and Huh-7 cells cocultured with $CD8^+$ T cells. **e,f,** Quantification of apoptotic rates of indicated Hep3B and Huh-7 cells cocultured with $CD8^+$ T cells. $n = 3$ independent experiments. Data are shown as mean ± SEM. Exact *P* values from top to bottom (**e**): 0.001196, 0.001051, 6.01E−05. Exact *P* values from top to bottom (**f**): 0.005506, 0.008871, 0.000501. **g-i,** Flow cytometry analysis of apoptotic rates of indicated Hep3B and Huh-7 cells with $CD8^+$ T cells coculture and methionine and leucine supplementation. $n = 3$ independent experiments. Data are shown as mean ± SEM. Exact *P* values from top to bottom (**g**): 0.001044, 0.000873, 0.006523. Exact *P* values from top to bottom (**h**): 0.001924, 0.001796, 0.018599. NS, not significant; **, $P < 0.01$; ***, $P < 0.001$ by two-tailed Student's T-test. Data are representative of at least three independent experiments.

**Supplementary Fig. 24: circPETH-147aa weakens specific anti-HCC response and correlates with immunotherapeutic effects for HCC patients, related to Fig. 4.**

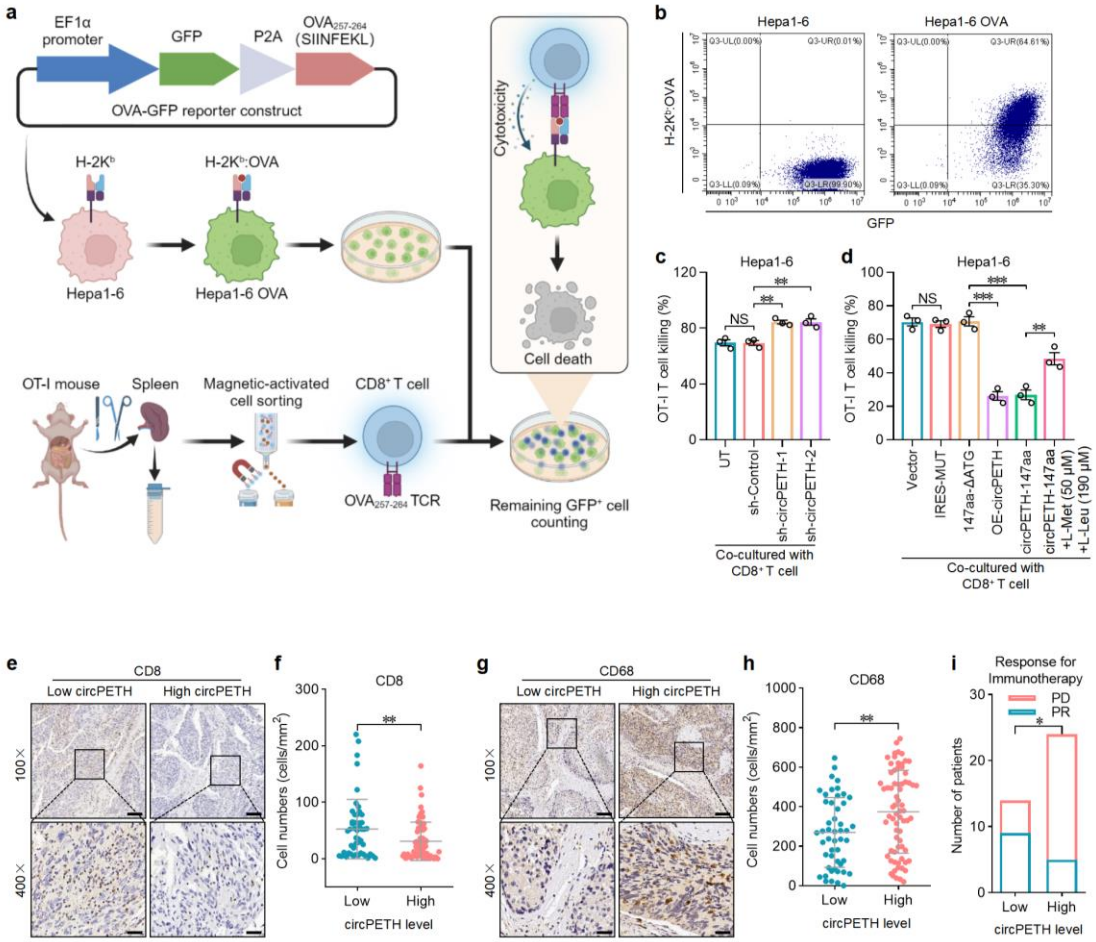


**a,** Schematic of the construction of Hepa1-6 OVA cells and the coculture with OT-I T cells [Created in BioRender. Cai, Y. (2024) https://BioRender.com/v84x844]. **b,** Flow cytometry analysis of H-2K$^b$:OVA expression levels on the surface of Hepa1-6 cells. **c,** Quantification of the percentages of Hepa1-6 OVA cells with circPETH knockdown killed by OT-I T cells. $n = 3$ independent experiments. Data are shown as mean ± SEM. Exact $P$ values from top to bottom: 0.006920, 0.002649. **d,** Quantification of the percentages of Hepa1-6 OVA cells with circPETH overexpression killed by OT-I T cells. $n = 3$ independent experiments. Data are shown as mean ± SEM. Exact $P$ values from top to bottom: 0.000400, 0.000296, 0.009778. **e,** Representative IHC staining of CD8 in HCC tissues for low and high circPETH groups. Scale bars from top to bottom: 200 μm, 50 μm. **f,** Statistical analysis of CD8$^+$ T cell numbers in HCC tissues for low and high circPETH groups. $n = 70$ for high circPETH group and $n = 50$ for low circPETH

group. Data are shown as mean ± SD. Exact *P* value: 0.007046. **g,** Representative IHC staining of CD68 in HCC tissues for low and high circPETH groups. Scale bars from top to bottom: 200 μm, 50 μm. **h,** Statistical analysis of TAMs numbers in HCC tissues for low and high circPETH groups. $n = 70$ for high circPETH group and $n = 50$ for low circPETH group. Data are shown as mean ± SD. Exact *P* value: 0.004687. **i,** Statistical analysis of patient numbers associated with different immunotherapeutic effects for low and high circPETH groups. $n = 24$ for high circPETH group and $n = 14$ for low circPETH group. Exact *P* value: 0.013796. NS, not significant; *, $P < 0.05$; **, $P < 0.01$; ***, $P < 0.001$ by two-tailed Student's T-test. Data are representative of at least three independent experiments.

**Supplementary Fig. 25: Norathyriol reverses circPETH-147aa-facilitated metabolic and metastatic phenotype acquisition of HCC cells, related to Fig. 5.**

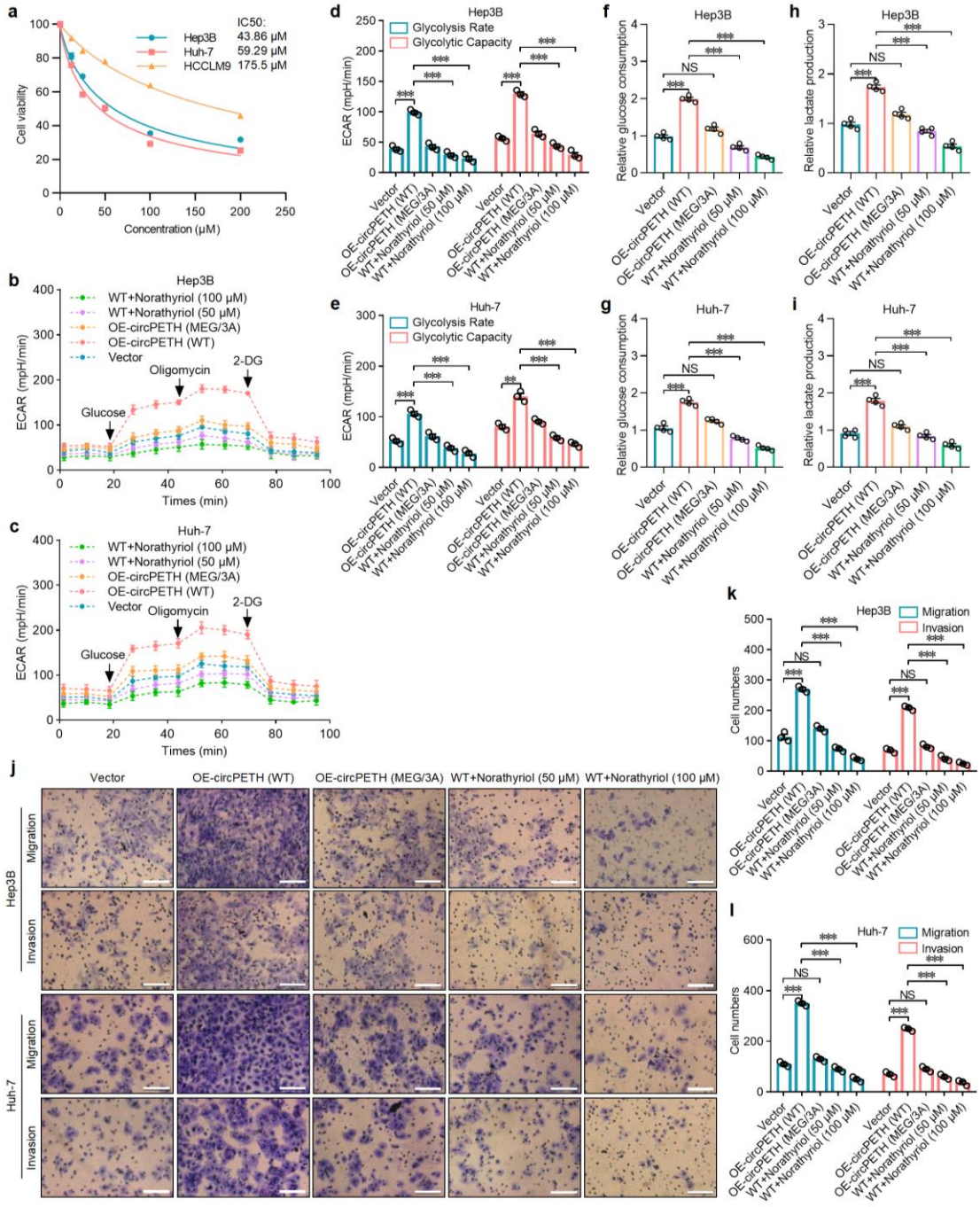


a, The IC50 for Hep3B, Huh-7 and HCCLM9 cells were determined by CCK-8 assays. **b,c,** ECARs of indicated Hep3B and Huh-7 cells treated with Norathyriol at different concentrations for 24 h. **d,e,** Glycolysis rates and glycolysis capacities of Hep3B and Huh-7 cells treated with Norathyriol at different concentrations for 24 h. $n = 3$ independent experiments. Data are shown as mean ± SEM. Exact $P$ values from top to bottom and left to right (**d**): 0.000145, 8.80E−05, 0.000193, 9.60E−05, 9.00E−05,

8.50E−05. Exact *P* values from top to bottom and left to right (**e**): 0.000387, 0.000380, 0.000875, 0.000212, 0.000341, 0.001281. **f,g,** Glucose consumption of indicated Hep3B and Huh-7 cells treated with Norathyriol at different concentrations for 24 h. $n = 4$ independent experiments. Data are shown as mean ± SEM. Exact *P* values from top to bottom (**f**): 9.03E−08, 5.54E−07, 3.03E−06. Exact *P* values from top to bottom (**g**): 4.52E−07, 1.99E−06, 5.74E−05. **h,i,** Lactate production of indicated Hep3B and Huh-7 cells treated with Norathyriol at different concentrations for 24 h. $n = 4$ independent experiments. Data are shown as mean ± SEM. Exact *P* values from top to bottom (**h**): 1.07E−06, 4.05E−06, 2.23E−05. Exact *P* values from top to bottom (**i**): 4.44E−06, 1.62E−05, 3.83E−05. **j-l,** The invasion and migration of indicated Hep3B and Huh-7 cells treated with Norathyriol at different concentrations for 24 h. Scale bar, 100 μm. $n = 3$ independent experiments. Data are shown as mean ± SEM. Exact *P* values from top to bottom and left to right (**j**): 4.93E−06, 1.11E−05, 0.000119, 4.08E−06, 1.58E−05, 2.33E−05. Exact *P* values from top to bottom and left to right (**k**): 3.28E−06, 5.80E−06, 7.98E−06, 9.15E−06, 1.32E−05, 1.63E−05. NS, not significant; ***, $P < 0.001$ by two-tailed Student's T-test. Data are representative of at least three independent experiments.

**Supplementary Fig. 26: Norathyriol strengthens tumour-killing effects of CD8$^+$ T cells and increases anti-PD1 efficacy, related to Fig. 6 and Fig. 7.**

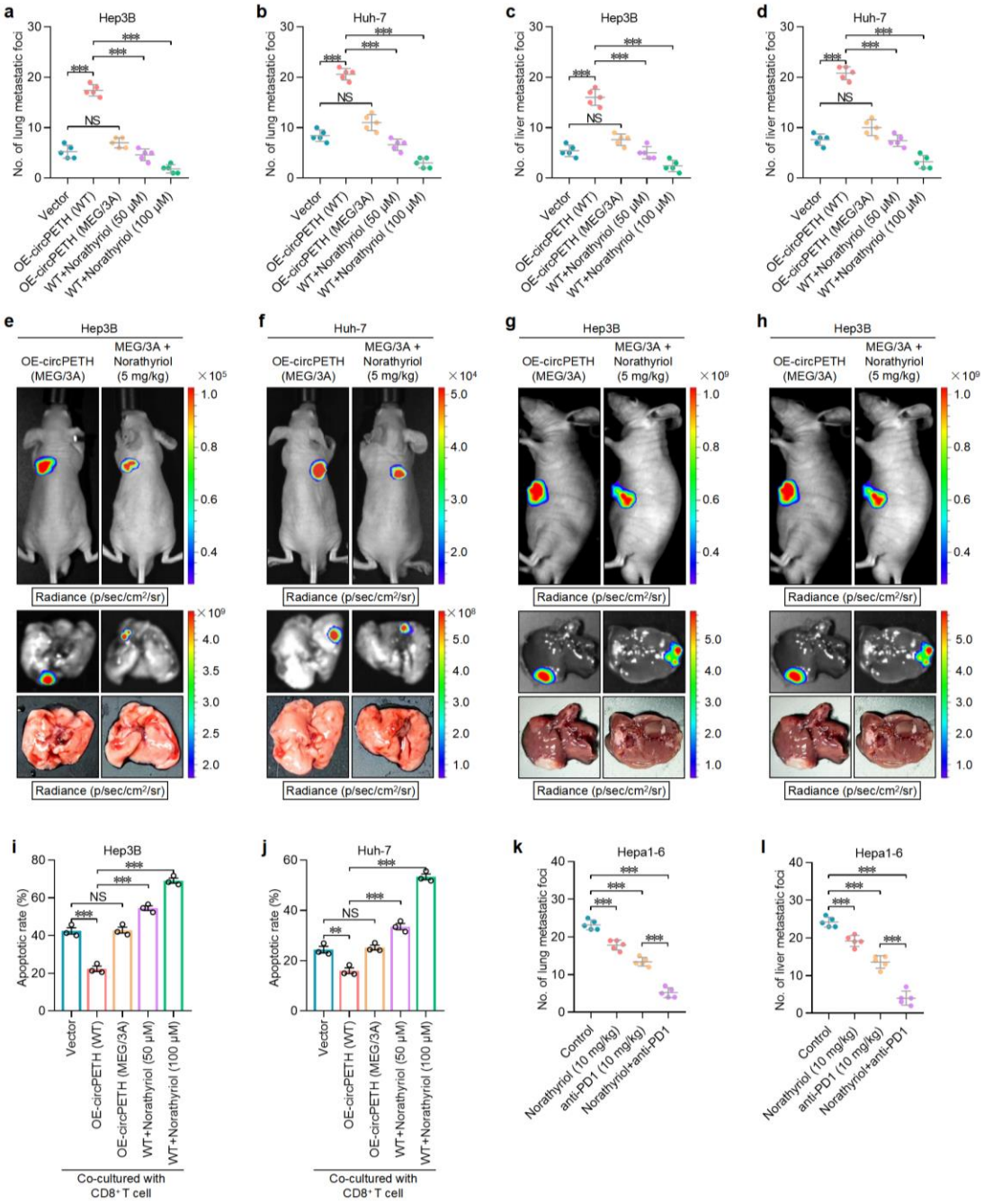


**a,b,** Statistical analysis of metastatic foci in the lung. $n = 5$ for each group. Data are shown as mean ± SD. Exact *P* values from top to bottom (**a**): 7.80E−09, 1.04E−07, 2.64E−07. Exact *P* values from top to bottom (**b**): 5.22E−09, 5.14E−08, 1.51E−07. **c,d,** Statistical analysis of metastatic foci in the liver. $n = 5$ for each group. Data are shown as mean ± SD. Exact *P* values from top to bottom (**c**): 2.84E−07, 1.78E−06, 1.94E−06. Exact *P* values from top to bottom (**d**): 2.44E−08, 1.27E−07, 1.43E−07. **e,f,**

Representative bioluminescence, fluorescence and brightfield photographs of the murine tail vein injection lung metastasis models with indicated Hep3B and Huh-7 cells. Norathyriol was intraperitoneally injected (5 mg/kg, once daily for two weeks). $n = 5$ for each group. **g,h,** Representative bioluminescence, fluorescence and brightfield photographs of intrahepatic metastatic nodules in liver orthotopic implanted intrahepatic metastasis models with indicated Hep3B and Huh-7 cells. Norathyriol was intraperitoneally injected (5 mg/kg, once daily for two weeks). $n = 5$ for each group. **i,j,** Quantification of apoptotic rates of indicated Hep3B and Huh-7 cells cocultured with $CD8^+$ T cells and treated with Norathyriol at different concentrations for 24 h. $n = 3$ independent experiments. Data are shown as mean ± SEM. Exact *P* values from top to bottom (**e**): 1.83E−05, 6.64E−05, 0.000835. Exact *P* values from top to bottom (**f**): 2.27E−05, 0.000494, 0.008502. **k,** Statistical analysis of metastatic foci in the lung. $n = 5$ for each group. Data are shown as mean ± SD. Exact *P* values from top to bottom: 2.05E−08, 1.43E−06, 0.000179, 5.54E−06. **l,** Statistical analysis of metastatic foci in the liver. $n = 5$ for each group. Data are shown as mean ± SD. Exact *P* values from top to bottom: 4.40E−08, 3.69E−06, 0.000475, 2.69E−05. NS, not significant; **, $P < 0.01$; ***, $P < 0.001$ by two-tailed Student's T-test. Data are representative of at least three independent experiments.

**Supplementary Fig. 27: Norathyriol boosts cytotoxic CD8$^+$ T-cell function in vivo, related to Fig. 7.**

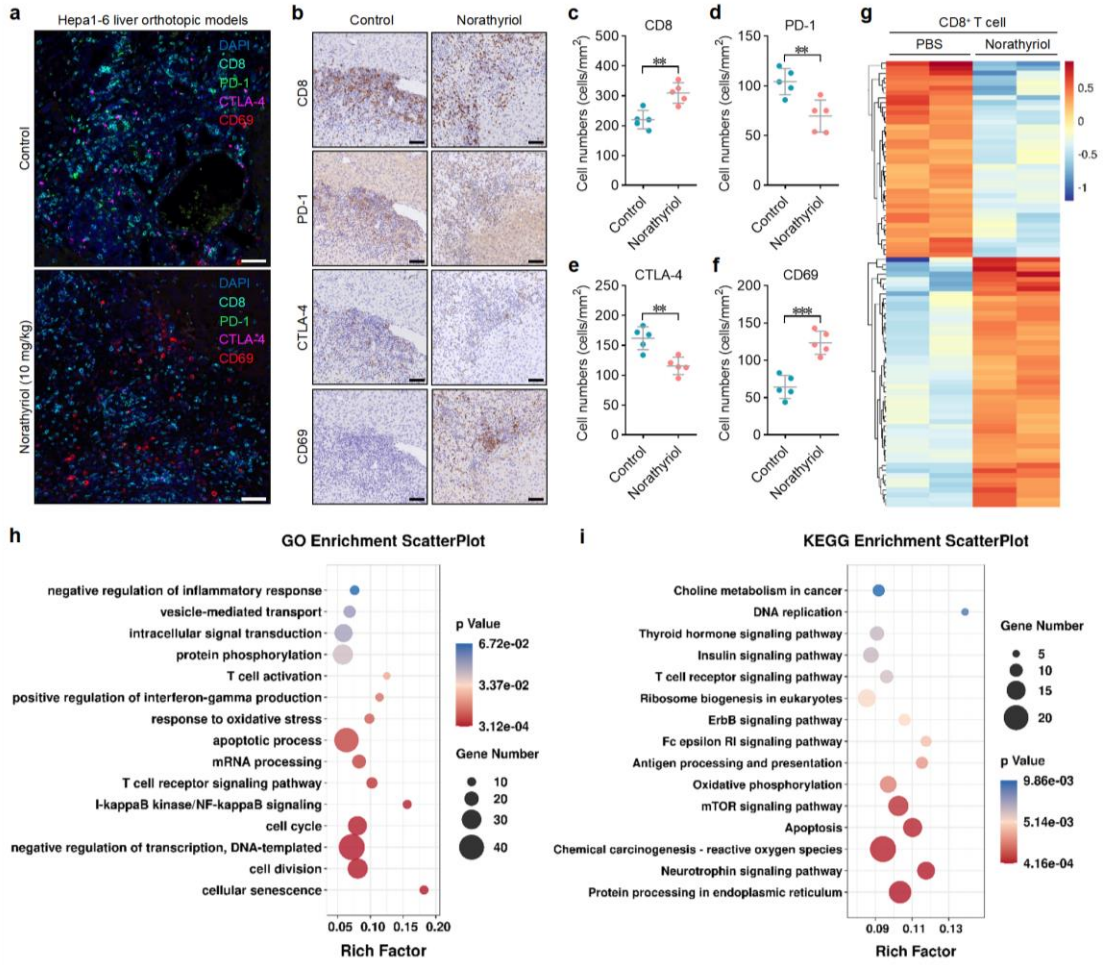


**a,** Representative IF staining of CD8, PD-1, TIM-3 and CTLA-4 in HCC tissues of Hepa1-6 liver orthotopic models. Norathyriol was intraperitoneally injected (10 mg/kg, once daily for two weeks). $n = 5$ for each group. Scale bar, 50 μm. **b,** Representative IHC staining of CD8, PD-1, TIM-3 and CTLA-4 in HCC tissues of Hepa1-6 liver orthotopic models. Norathyriol was intraperitoneally injected (10 mg/kg, once daily for two weeks). $n = 5$ for each group. Scale bar, 50 μm. **c,** Statistical analysis of CD8$^+$ cell numbers in HCC tissues of Hepa1-6 liver orthotopic models. $n = 5$ for each group. Data are shown as mean ± SD. Exact $P$ value: 0.002538. **d,** Statistical analysis of PD-1$^+$ cell numbers in HCC tissues of Hepa1-6 liver orthotopic models. $n = 5$ for each group. Data are shown as mean ± SD. Exact $P$ value: 0.005888. **e,** Statistical analysis of CTLA-4$^+$ cell numbers in HCC tissues of Hepa1-6 liver orthotopic models. $n = 5$ for each group. Data are shown as mean ± SD. Exact $P$ value: 0.002587. **f,** Statistical analysis of CD69$^+$

cell numbers in HCC tissues of Hepa1-6 liver orthotopic models. $n = 5$ for each group. Data are shown as mean ± SD. Exact $P$ value: 0.000306. **g,** Heatmap of differentially expressed genes in Norathyriol versus PBS treated $CD8^+$ T cells by RNA-seq. **h,i,** GO and KEGG analysis of the differentially expressed genes in RNA-seq. **, $P < 0.01$; ***, $P < 0.001$ by two-tailed Student's T-test. Data are representative of at least three independent experiments.

**Supplementary Fig. 28: Norathyriol boosts cytotoxic CD8$^+$ T-cell function in vitro, related to Fig. 7.**

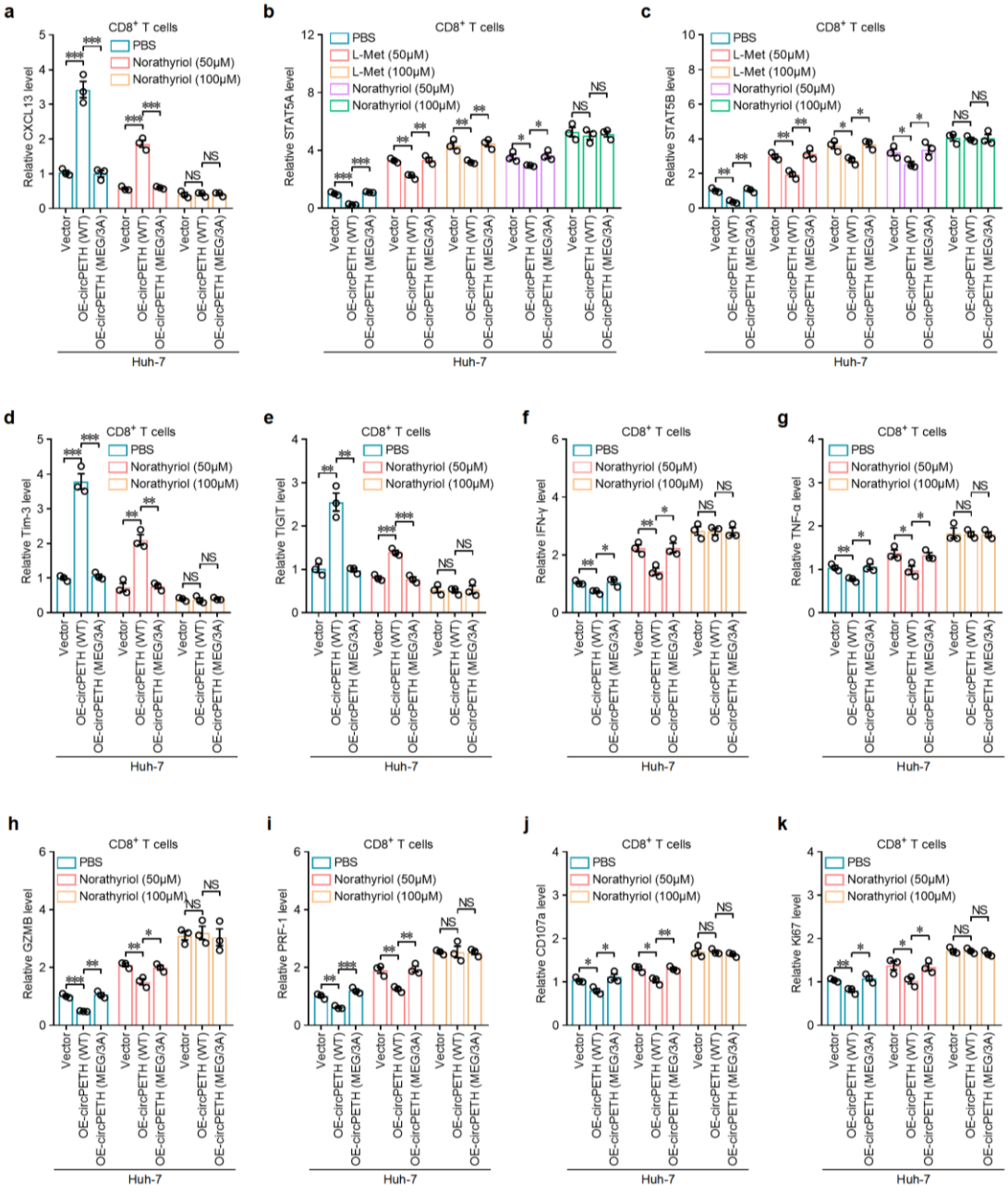


**a,** CXCL13 expression in CD8$^+$ T cells with indicated Huh-7 cells coculture and Norathyriol treatment at different concentrations for 24 h. $n = 3$ independent experiments. Data are shown as mean ± SEM. Exact *P* values from left to right: 0.000600, 0.000671, 0.000268, 0.000246. **b,** STAT5A expression in CD8$^+$ T cells with indicated Huh-7 cells coculture and Norathyriol or methionine treatment at different concentrations for 24 h. $n = 3$ independent experiments. Data are shown as mean ± SEM.

Exact *P* values from left to right: 0.000326, 5.04E−06, 0.001355, 0.004338, 0.009872, 0.003978, 0.039376, 0.023066. **c,** STAT5B expression in $CD8^+$ T cells with indicated Huh-7 cells coculture and Norathyriol or methionine treatment at different concentrations for 24 h. $n = 3$ independent experiments. Data are shown as mean ± SEM. Exact *P* values from left to right: 0.001365, 0.001536, 0.004213, 0.006207, 0.017703, 0.010255, 0.048853, 0.046352. **d,** Tim-3 expression in $CD8^+$ T cells with indicated Huh-7 cells coculture and Norathyriol treatment at different concentrations for 24 h. $n = 3$ independent experiments. Data are shown as mean ± SEM. Exact *P* values from left to right: 0.000253, 0.000286, 0.001903, 0.001109. **e,** TIGIT expression in $CD8^+$ T cells with indicated Huh-7 cells coculture and Norathyriol treatment at different concentrations for 24 h. $n = 3$ independent experiments. Data are shown as mean ± SEM. Exact *P* values from left to right: 0.002639, 0.001832, 0.000622, 0.000788. **f,** IFN-γ expression in $CD8^+$ T cells with indicated Huh-7 cells coculture and Norathyriol treatment at different concentrations for 24 h. $n = 3$ independent experiments. Data are shown as mean ± SEM. Exact *P* values from left to right: 0.005802, 0.023795, 0.008786, 0.015365. **g,** TNF-α expression in $CD8^+$ T cells with indicated Huh-7 cells coculture and Norathyriol treatment at different concentrations for 24 h. $n = 3$ independent experiments. Data are shown as mean ± SEM. Exact *P* values from left to right: 0.006534, 0.014662, 0.039378, 0.040725. **h,** GZMB expression in $CD8^+$ T cells with indicated Huh-7 cells coculture and Norathyriol treatment at different concentrations for 24 h. $n = 3$ independent experiments. Data are shown as mean ± SEM. Exact *P* values from left to right: 0.000302, 0.001246, 0.007557, 0.019074. **i,** PRF-1 expression in $CD8^+$ T cells with indicated Huh-7 cells coculture and Norathyriol treatment at different concentrations for 24 h. $n = 3$ independent experiments. Data are shown as mean ± SEM. Exact *P* values from left to right: 0.003059, 0.000889, 0.005094, 0.003832. **j,** CD107a expression in $CD8^+$ T cells with indicated Huh-7 cells coculture and Norathyriol treatment at different concentrations for 24 h. $n = 3$ independent experiments. Data are shown as mean ± SEM. Exact *P* values from left to right: 0.014853, 0.020880, 0.012140, 0.008637. **k,** Ki67 expression in $CD8^+$ T cells with indicated Huh-7 cells coculture and Norathyriol treatment at different

concentrations for 24 h. $n = 3$ independent experiments. Data are shown as mean ± SEM. Exact $P$ values from left to right: 0.007043, 0.017086, 0.038944, 0.038003. NS, not significant; *, $P < 0.05$; **, $P < 0.01$; ***, $P < 0.001$ by two-tailed Student's T-test. Data are representative of at least three independent experiments.

**Supplementary Fig. 29: Flow cytometry analysis of PD-1, CTLA-4 and Tim-3 expressions on CD8$^+$ T-cell surface, related to Fig. 7.**

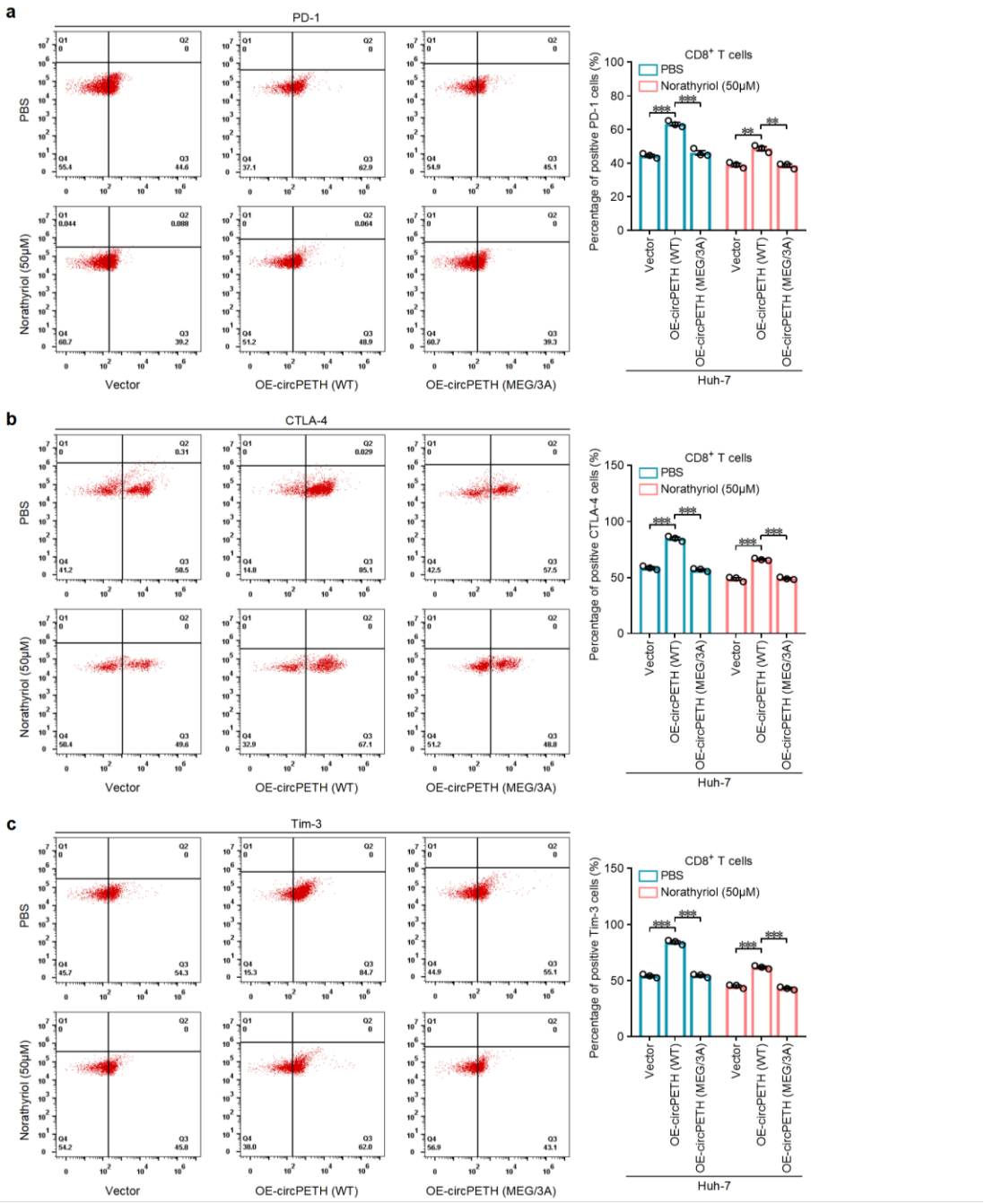


**a,** Flow cytometry analysis of PD-1 expression on CD8$^+$ T cells with indicated Huh-7 cells coculture and Norathyriol treatment for 24 h. $n = 3$ independent experiments. Data are shown as mean ± SEM. Exact $P$ values from left to right: 0.000132, 0.000376, 0.003434, 0.002797. **b,** Flow cytometry analysis of CTLA-4 expression on CD8$^+$ T cells with indicated Huh-7 cells coculture and Norathyriol treatment for 24 h. $n = 3$ independent experiments. Data are shown as mean ± SEM. Exact $P$ values from left to

right: 7.62E−05, 5.07E−05, 0.000196, 3.71E−05. **c,** Flow cytometry analysis of Tim-3 expression on $CD8^+$ T cells with indicated Huh-7 cells coculture and Norathyriol treatment for 24 h. $n = 3$ independent experiments. Data are shown as mean ± SEM. Exact *P* values from left to right: 3.09E−05, 2.96E−05, 0.000199, 6.85E−05. NS, not significant; **, $P < 0.01$; ***, $P < 0.001$ by two-tailed Student's T-test. Data are representative of at least three independent experiments.

**Supplementary Fig. 30: Flow cytometry analysis of TIGIT, IFN-γ and GZMB expressions on CD8$^+$ T-cell surface, related to Fig. 7.**

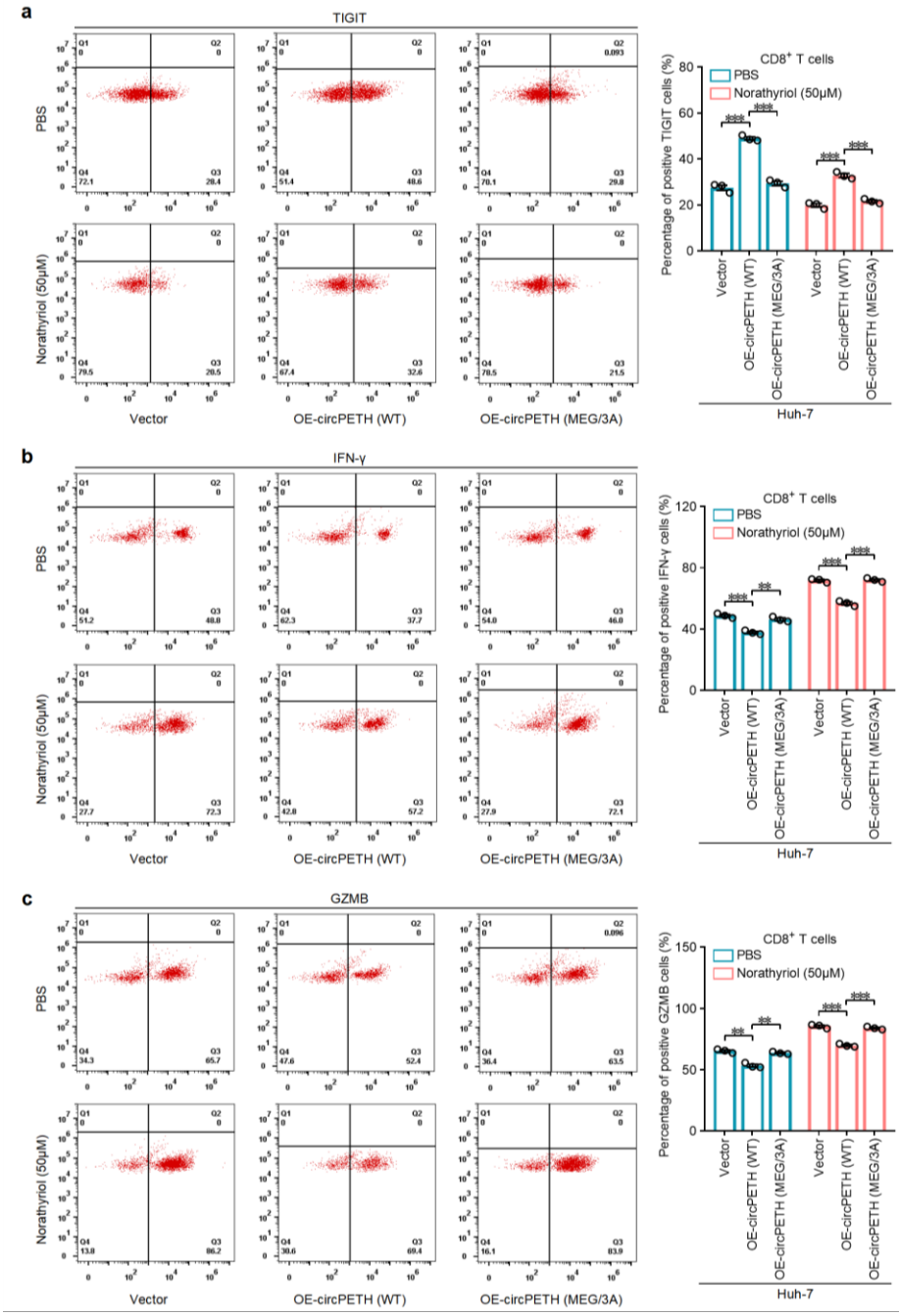


**a,** Flow cytometry analysis of TIGIT expression on CD8$^+$ T cells with indicated Huh-7 cells coculture and Norathyriol treatment for 24 h. $n = 3$ independent experiments. Data are shown as mean ± SEM. Exact $P$ values from left to right: 7.97E−05, 6.99E−05, 0.000380, 0.000382. **b,** Flow cytometry analysis of IFN-γ expression on CD8$^+$ T cells with indicated Huh-7 cells coculture and Norathyriol treatment for 24 h. $n = 3$ independent experiments. Data are shown as mean ± SEM. Exact $P$ values from left to

right: 0.000522, 0.001799, 0.000240, 0.000215. **c,** Flow cytometry analysis of GZMB expression on $CD8^+$ T cells with indicated Huh-7 cells coculture and Norathyriol treatment for 24 h. $n = 3$ independent experiments. Data are shown as mean ± SEM. Exact *P* values from left to right: 0.001294, 0.001252, 0.000164, 0.000133. NS, not significant; **, $P < 0.01$; ***, $P < 0.001$ by two-tailed Student's T-test. Data are representative of at least three independent experiments.

**Supplementary Fig. 31: Gating Strategies (Flow cytometry). Representative flow cytometry data with gating strategies.**

**a** The Gating stategy for Supplementary Fig. 1b

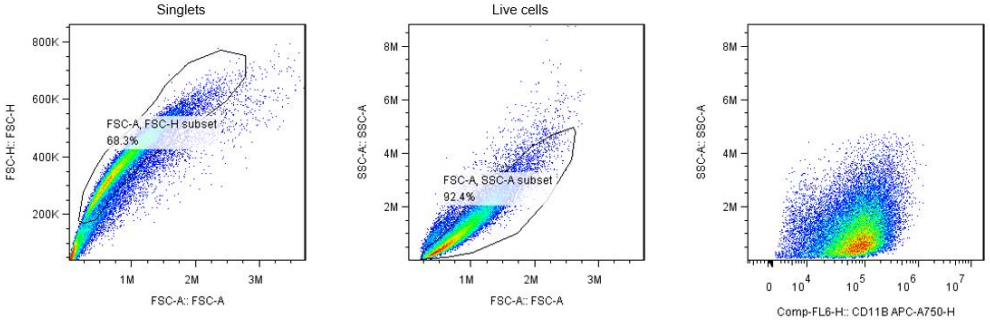


**b** The Gating stategy for Supplementary Fig. 22a

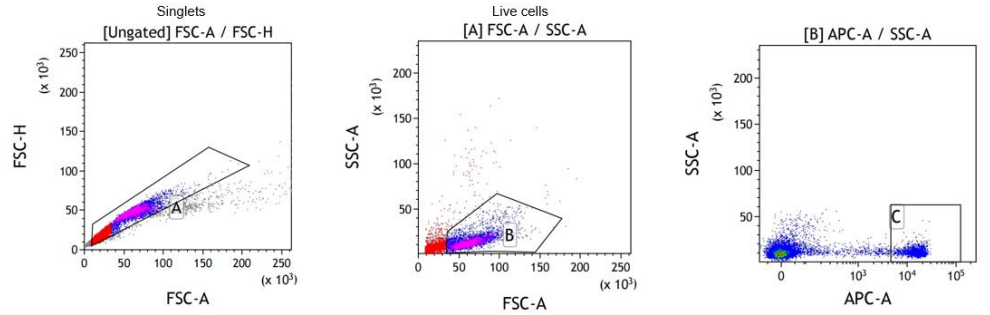


**c** The Gating stategy for Supplementary Fig. 22d

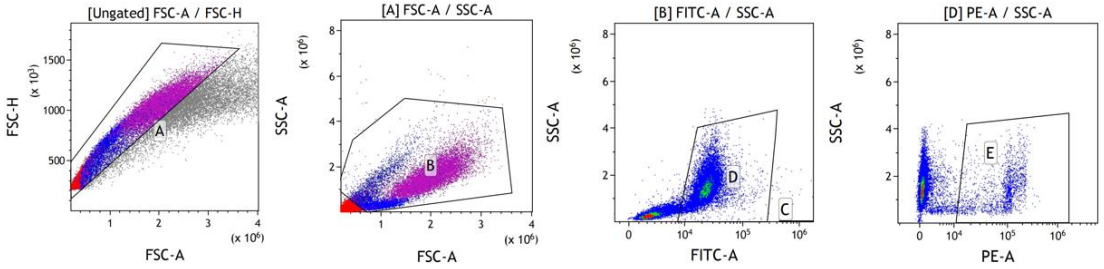


**d** The Gating stategy for Supplementary Fig. 22i

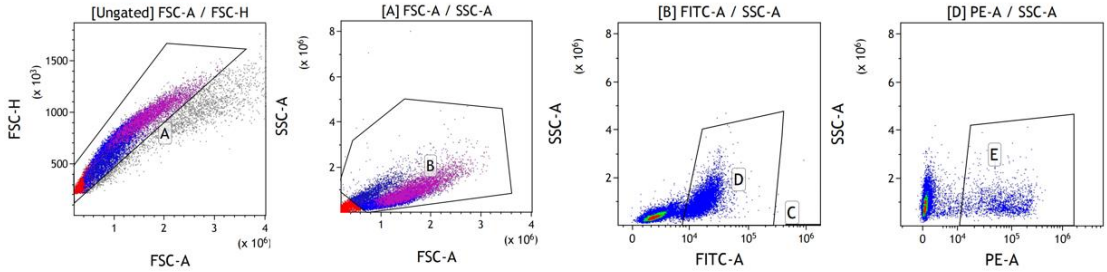

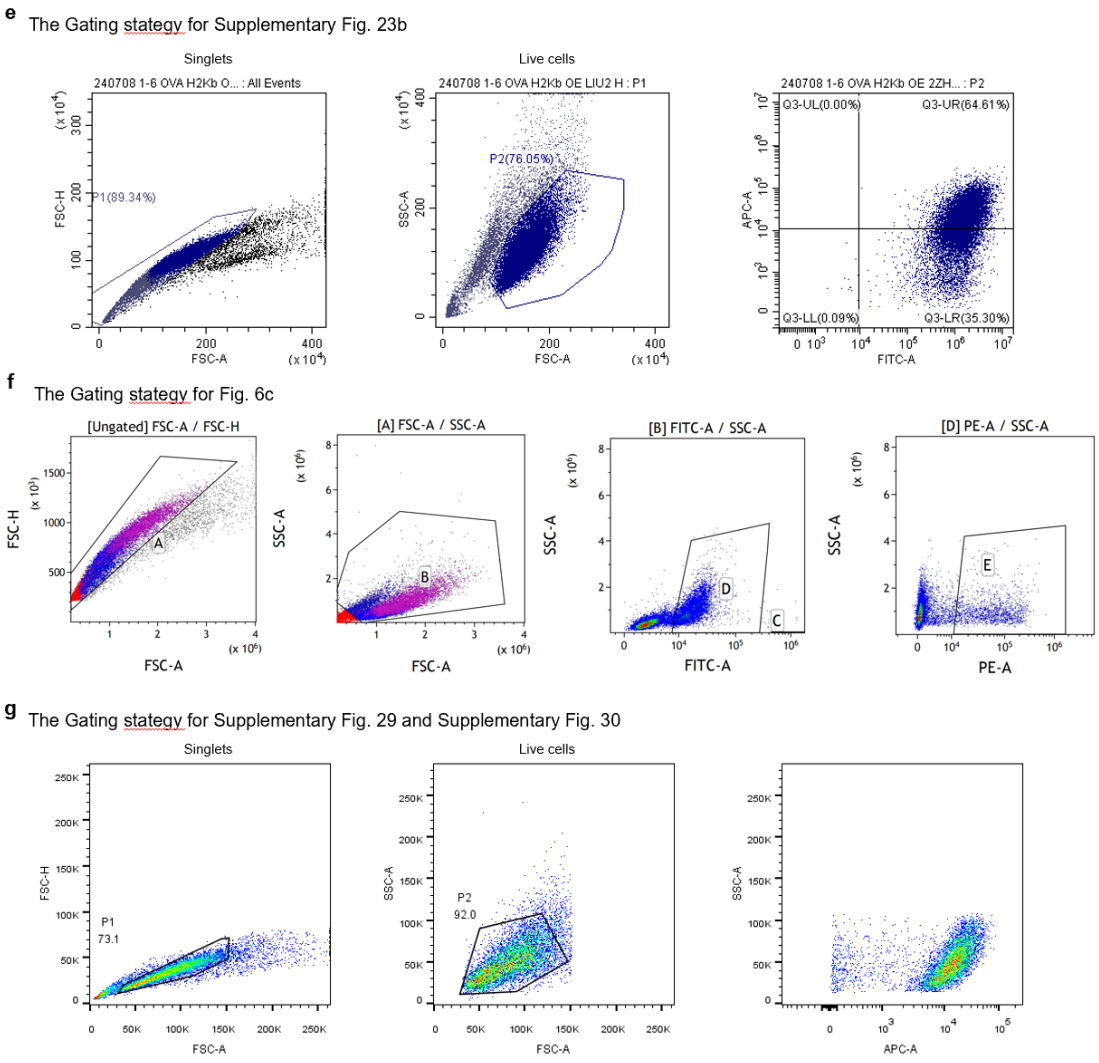


**a,** Representative flow cytometry data with gating strategy for Supplementary Fig. 1b. **b,** Representative flow cytometry data with gating strategy for Supplementary Fig. 22a. **c,** Representative flow cytometry data with gating strategy for Supplementary Fig. 22d. **d,** Representative flow cytometry data with gating strategy for Supplementary Fig. 22i. **e,** Representative flow cytometry data with gating strategy for Supplementary Fig. 23b. **f,** Representative flow cytometry data with gating strategy for Fig. 6c. **g,** Representative flow cytometry data with gating strategy for Supplementary Fig. 29 and Supplementary Fig. 30. Data are representative of at least three independent experiments.

**Supplementary Tables**

| **Supplementary Table 1. Clinical characteristics of 120 HCC patients according to circPETH expression level** | | | |
|---|---|---|---|
| **Variables** | **High circPETH (n = 70)** | **Low circPETH (n = 50)** | ***P* value** |
| Age, year, >60/⩽60 | 18/52 | 9/41 | 0.3184 |
| Gender, male/female | 60/10 | 44/6 | 0.7165 |
| HbsAg, positive/negative | 63/7 | 47/3 | 0.6551 |
| Liver cirrhosis, present/absent | 45/25 | 31/19 | 0.7978 |
| AFP, μg/L, >20/⩽20 | 45/25 | 38/12 | 0.1707 |
| Tumor size, cm, >5/⩽5 | 48/22 | 24/26 | **0.0233** |
| Tumor number, multiple/solitary | 24/46 | 7/43 | **0.0123** |
| Microvascular invasion, present/absent | 41/29 | 15/35 | **0.0020** |
| Macrovascular invasion, present/absent | 4/66 | 3/47 | 0.7420 |
| Differentiation, poor/well-moderate | 26/44 | 22/28 | 0.4497 |
| TNM stage, II+III/I | 41/29 | 16/34 | **0.0041** |
| BCLC stage, B+C/A | 34/36 | 11/39 | **0.0030** |

**Chi-square tests were performed to analyze the correlation between gene expression and clinical characteristics.**

**Statistically significant p values are shown in bold.**

| Supplementary Table 2. Prognostic factors for overall survival and recurrence-free survival by the univariate Cox proportional hazards regression model | | | | | | |
|---|---|---|---|---|---|---|
| **Variables** | **Overall survival** | | | **Recurrence-free survival** | | |
| | **HR** | **95% CI** | ***P* value** | **HR** | **95% CI** | ***P* value** |
| Age, year, >60/⩽60 | 0.648 | 0.363-1.160 | 0.144 | 0.592 | 0.310-1.132 | 0.113 |
| Gender, male/female | 1.025 | 0.526-1.999 | 0.942 | 0.807 | 0.369-1.769 | 0.593 |
| HbsAg, positive/negative | 0.494 | 0.236-1.037 | 0.062 | 0.561 | 0.255-1.235 | 0.151 |
| Liver cirrhosis, present/absent | 0.844 | 0.530-1.343 | 0.473 | 0.794 | 0.486-1.298 | 0.357 |
| AFP, μg/L, >20/⩽20 | 0.776 | 0.480-1.255 | 0.301 | 0.694 | 0.420-1.147 | 0.154 |
| Tumor size, cm, >5/⩽5 | 1.299 | 0.810-2.082 | 0.278 | 0.970 | 0.595-1.581 | 0.903 |
| Tumor number, multiple/solitary | 1.783 | 1.090-2.916 | **0.021** | 1.518 | 0.889-2.592 | 0.126 |
| Microvascular invasion, present/absent | 1.870 | 1.185-2.949 | **0.007** | 1.806 | 1.124-2.903 | **0.015** |
| Macrovascular invasion, present/absent | 2.469 | 1.066-5.717 | **0.035** | 2.345 | 1.009-5.448 | **0.048** |
| Differentiation, poor/well-moderate | 1.105 | 0.638-1.616 | 0.949 | 1.122 | 0.694-1.815 | 0.638 |
| TNM stage, II+III/I | 1.768 | 1.120-2.790 | **0.014** | 1.719 | 1.069-2.764 | **0.025** |
| BCLC stage, B+C/A | 1.896 | 1.201-2.993 | **0.006** | 1.693 | 1.050-2.730 | **0.031** |
| circPETH expression (high/low) | 2.161 | 1.549-3.015 | **0.0003** | 2.087 | 1.502-2.901 | **0.0005** |
| **HR, hazard ratio; CI, confidence interval.** | | | | | | |

**Univariate analyses of the Cox proportional-hazards model were performed to identify independent prognostic risk factors.**

**Statistically significant p values are shown in bold.**

| Supplementary Table 3. Independent prognostic factors for overall survival and recurrence-free survival by the multivariate Cox proportional hazards regression model | | | | | | |
|---|---|---|---|---|---|---|
| **Variables** | **Overall survival** | | | **Recurrence-free survival** | | |
| | **HR** | **95% CI** | ***P* value** | **HR** | **95% CI** | ***P* value** |
| Tumor number, multiple/solitary | 1.168 | 0.680-2.008 | 0.573 | | | |
| Microvascular invasion, present/absent | 1.587 | 0.945-2.665 | 0.080 | 1.869 | 0.957-3.650 | 0.067 |
| Macrovascular invasion, present/absent | 1.921 | 0.803-4.596 | 0.143 | 1.739 | 0.677-4.471 | 0.251 |
| TNM stage, II+III/I | 1.411 | 0.622-1.937 | 0.163 | 1.293 | 0.727-2.300 | 0.381 |
| BCLC stage, B+C/A | 1.702 | 1.064-2.721 | **0.027** | 1.478 | 0.891-2.451 | 0.130 |
| circPETH expression (high/low) | 1.797 | 1.244-2.595 | **0.002** | 1.752 | 1.197-2.565 | **0.004** |
| **Potential confounders with P values less than 0.05 in univariate regression analyses were selected into multivariate regression models. HR, hazard ratio; CI, confidence interval.** | | | | | | |

**Multivariate analyses of the Cox proportional-hazards model were performed to identify independent prognostic risk factors.**

**Statistically significant p values are shown in bold.**

| Supplementary Table 4. Sequence of circPETH DNA probe used in this study | |
|---|---|
| **Name** | **Sequence** |
| circPETH DNA probe | digoxin-<br>TCACAGAGGCTGAGGCTGCAGTGGCCACCCAGGAGACATCCACCGTCAGGCTAAAGGTCAG<br>CTCCACAGCCGTAAGGACACAGCACACAACCACCCGACCTGTTCCCGACACCTCCCGGCTGC<br>CTGGGGCCACCCCTGGGCTCACCACGGTGGAGATAGTGACAATGTCTCACCAAGGACAAAGT<br>ATTTTGGACAGATATCATCAACGAAGCCATTTTCAGTGCCAACCGCCTCACAGGTTCCGATGT<br>CAACTTGTTGGCTGAAAACCTACTGTCCCCAGAGGATATGGTTCTCTTCCACAACCTCACCCA<br>GCCAAGAGGAGTGAACTGGTGTGAGAGG-digoxin |

**Supplementary Table 5.** Small molecule screening data

| Category | Parameter | Description |
|---|---|---|
| Assay | Type of assay | Virtual screening and *in vitro* |
| | Target | circPETH-147aa |
| | Primary measurement | Detection of docking score, protein stability and dissociation constant |
| | Key reagents | Purified recombinant circPETH-147aa protein |
| | Assay protocol | The section in the methods of the paper that describes the assay protocol, including virtual screening and nano differential scanning fluorimetry (nanoDSF), and surface plasmon resonance (SPR) |
| | Additional comments | |
| Library | Library size | 40,000 small molecules |
| | Library composition | Known bioactives, natural products, drug-like molecules |
| | Source | TargetMol library (bioactive compound library, Target Molecule Corp) |
| | Additional comments | |
| Screen | Format | Virtual screening, nanoDSF and SPR |
| | Concentration(s) tested | 100 μg/ml |
| | Plate controls | N/A |
| | Reagent/ compound dispensing system | Purified recombinant circPETH-147aa protein and small molecules |
| | Detection instrument and software | Protein stability analytic system Prometheus NT.48 and BIAcore X100 system |
| | Assay validation/QC | Standard deviation of controls |
| | Correction factors | Binding to reference |
| | Normalization | Full sensorgram using Biacore Evaluation software |
| | Additional comments | |
| Post-HTS analysis | Hit criteria | Docking score in Virtual screening < -5kcal/mo |
| | Hit rate | 0.305% |
| | Additional assay(s) | nanoDSF and SPR |
| | Confirmation of hit purity and structure | Compounds were repurchased |
| | Additional comments | |

**English Editing Certificate**

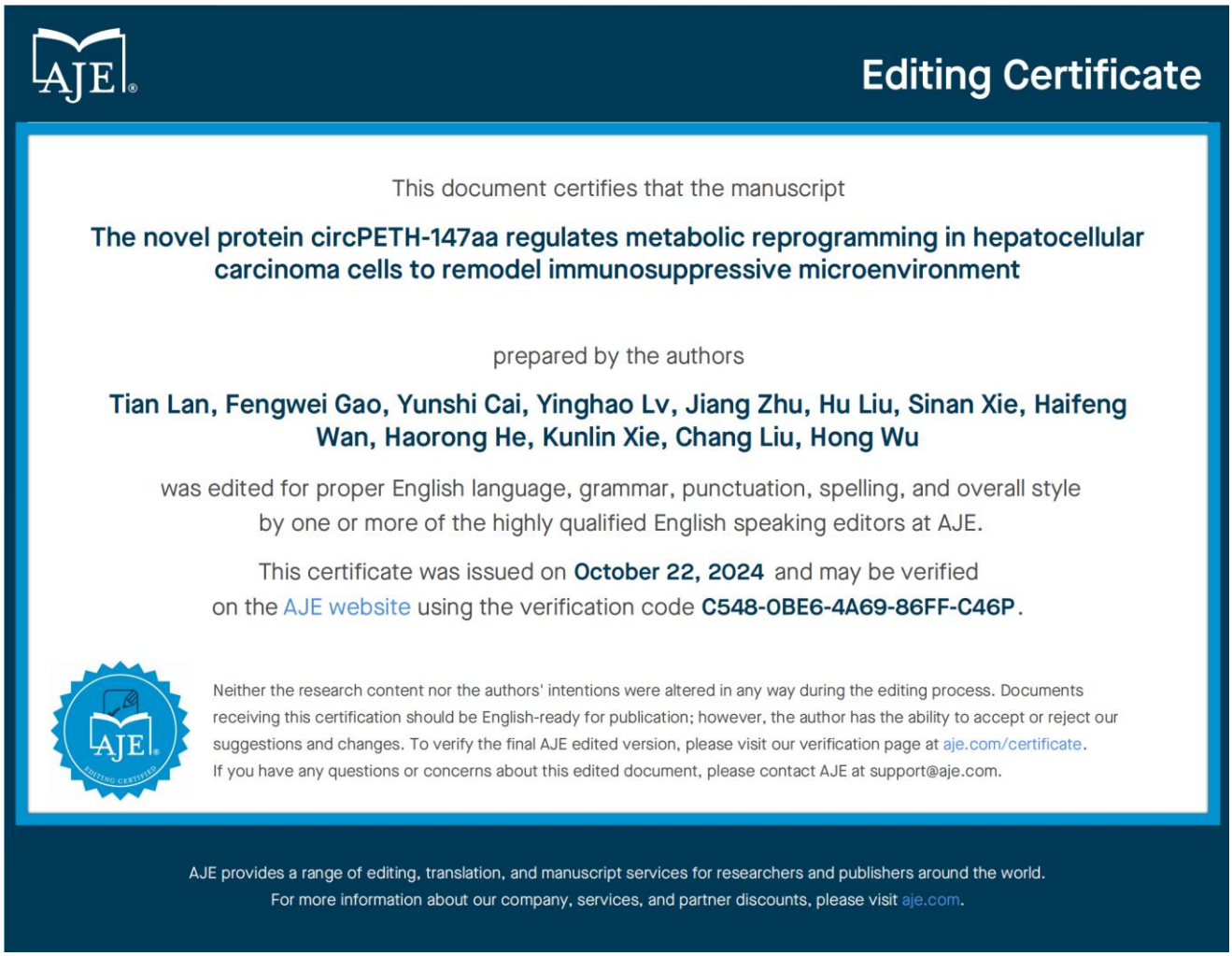

AJE

Editing Certificate

This document certifies that the manuscript

**The novel protein circPETH-147aa regulates metabolic reprogramming in hepatocellular carcinoma cells to remodel immunosuppressive microenvironment**

prepared by the authors

**Tian Lan, Fengwei Gao, Yunshi Cai, Yinghao Lv, Jiang Zhu, Hu Liu, Sinan Xie, Haifeng Wan, Haorong He, Kunlin Xie, Chang Liu, Hong Wu**

was edited for proper English language, grammar, punctuation, spelling, and overall style by one or more of the highly qualified English speaking editors at AJE.

This certificate was issued on **October 22, 2024** and may be verified on the AJE website using the verification code **C548-0BE6-4A69-86FF-C46P**.

Neither the research content nor the authors' intentions were altered in any way during the editing process. Documents receiving this certification should be English-ready for publication; however, the author has the ability to accept or reject our suggestions and changes. To verify the final AJE edited version, please visit our verification page at aje.com/certificate. If you have any questions or concerns about this edited document, please contact AJE at support@aje.com.

AJE provides a range of editing, translation, and manuscript services for researchers and publishers around the world. For more information about our company, services, and partner discounts, please visit aje.com.